

Development

AP2 Regulates Thickveins Trafficking to Attenuate NMJ Growth Signaling in *Drosophila*

Saumitra Dey Choudhury,^{1,*} Manish Kumar Dwivedi,^{1,*}  Srikanth Pippadpally,¹ Abhinandan Patnaik,¹ Shirish Mishra,² Raghu Padinjat,² and  Vimlesh Kumar¹

<https://doi.org/10.1523/ENEURO.0044-22.2022>

¹Department of Biological Sciences, Indian Institute of Science Education and Research (IISER) Bhopal, Bhopal, Madhya Pradesh 462 066, India and ²National Centre for Biological Sciences, Bangalore, Karnataka 560065, India

Abstract

Compromised endocytosis in neurons leads to synapse overgrowth and altered organization of synaptic proteins. However, the molecular players and the signaling pathways which regulate the process remain poorly understood. Here, we show that σ 2-adaptin, one of the subunits of the AP2-complex, genetically interacts with Mad, Medea and Dad (components of BMP signaling) to control neuromuscular junction (NMJ) growth in *Drosophila*. Ultrastructural analysis of σ 2-adaptin mutants show an accumulation of large vesicles and membranous structures akin to endosomes at the synapse. We found that mutations in σ 2-adaptin lead to an accumulation of Tkv receptors at the presynaptic membrane. Interestingly, the level of small GTPase Rab11 was significantly reduced in the σ 2-adaptin mutant synapses. However, expression of Rab11 does not restore the synaptic defects of σ 2-adaptin mutations. We propose a model in which AP2 regulates Tkv internalization and endosomal recycling to control synaptic growth.

Key words: σ 2-adaptin; BMP receptors; Rab11; synaptic growth; Thickveins

Significance Statement

Understanding the regulation of synaptic development and refinement could provide mechanistic insights into the neural basis of fundamental processes such as learning, memory and adaptation. In this study, we describe the role of σ 2-adaptin in attenuating neuromuscular junction (NMJ) growth signaling and show its involvement in the trafficking of Thickveins receptor at the *Drosophila* NMJ. σ 2-Adaptin interacts genetically with the BMP pathway components and NMJ synapses lacking σ 2-adaptin show reduced levels of the endosomal recycling marker, Rab11. Our study contributes to a broader understanding of AP2 complex-dependent regulation of synaptic growth signaling, which might have implications in neurodevelopment under conditions where endocytosis and trafficking of the BMP receptors are perturbed.

Introduction

Synapse development and refinement is an interplay of multiple signaling pathways, namely, the Bone morphogenetic protein (BMP), Wingless (Wnt), and Ubiquitin-Proteasome-mediated protein degradation (Highwire-Wallenda) pathways (McCabe et al., 2003, 2004; Franco et al., 2004; Collins et al., 2006; Ball et al., 2010; Budnik and Salinas, 2011; Piccioli and Littleton, 2014; Choudhury et al., 2016). Besides, there

are also pathways mediated by endocytic, cytoskeletal, and actin regulatory proteins (Franco et al., 2004; Piccioli and Littleton, 2014; Choudhury et al., 2016). Understanding the crosstalk among them is crucial to our understanding of the processes that regulate synapse development, refinement, and plasticity (Deshpande and Rodal, 2016). BMP signaling pathway at the *Drosophila* neuromuscular junction (NMJ) synapses is a well-studied growth-promoting pathway

Received January 27, 2022; accepted September 23, 2022; First published September 30, 2022.

The authors declare no competing financial interests.

Author contributions: S.D.C. and V.K. designed research; S.D.C., M.K.D., S.P., A.P., S.M., and V.K. performed research; R.P. contributed unpublished reagents/analytic tools; S.D.C. and V.K. analyzed data; S.D.C., S.P., and V.K. wrote the paper.

(Marqués et al., 2002; McCabe et al., 2003; O'Connor-Giles et al., 2008; Ball et al., 2010). The canonical BMP signaling is dependent on phosphorylated Smad (pMad in *Drosophila*) and its translocation into the motor neuron nuclei, followed by the transcription of BMP target genes (Keshishian and Kim, 2004; O'Connor-Giles et al., 2008; Ball et al., 2010; Kim and Marqués, 2012; Sulkowski et al., 2016; Vuilleumier et al., 2019).

At the *Drosophila* NMJ, the retrograde BMP signaling is initiated by secretion of Glass bottom boat (Gbb) from the muscle and the motor neurons (Goold and Davis, 2007). Gbb binds to Wit (a Type II receptor) as well as Tkv and Sax (Type I receptors) at the presynaptic nerve terminals to control NMJ growth and function (Aberle et al., 2002; Marqués et al., 2002; McCabe et al., 2003). Gbb binding to Wit triggers the tetramerization of BMP receptors that, in turn, phosphorylates the Smad transcription factor, Mothers against decapentaplegic (Mad). Following BMP activation, these receptors are endocytosed for retrograde transport to the motor neuron nuclei in the soma (Rodal et al., 2011; Smith et al., 2012; Vanlandingham et al., 2013).

Multiple studies have shown a tight correlation between defective endocytosis, altered synapse growth, and elevated synaptic pMad levels, implicating increased BMP signaling in synaptic development (O'Connor-Giles et al., 2008; Ball et al., 2010; Nahm et al., 2010; Shi et al., 2013; Piccioli and Littleton, 2014). One such study has shown that Nwk, an F-BAR and SH3 domain-containing protein that negatively regulates synaptic growth, interacts with Tkv along with Dap160 and Dynamin (both endocytic proteins) to attenuate retrograde BMP signaling during NMJ growth (O'Connor-Giles et al., 2008). Endocytic and endosomal pathways are, therefore, critical to controlling both the activity and localization of signaling proteins that regulate synaptic growth (Rodal et al., 2011; Cosker and Segal, 2014). Defects in intracellular trafficking can also lead to enhanced signaling from the cellular compartments (like endosomes), affecting the synapse

development (Di Fiore and De Camilli, 2001; Dubois et al., 2001; Sweeney and Davis, 2002; Rodal et al., 2011). In the neuronal context, the efficacy of intercellular signaling is regulated by the trafficking of activated receptor/ligand complexes following endocytosis from the presynaptic membrane.

Tightly regulated endocytic transport of BMP receptors relies on the spatiotemporal regulation of Rab GTPase function (Kelly et al., 2012). The Rab-family of GTPases regulates the progression of receptor endocytosis and participates in the successive steps of membrane maturation, receptor transport, and turnover (Horgan and McCaffrey, 2011). In particular, Rab5 regulates vesicle formation and is associated with early endosomes, while Rab7 and Rab11 associate with late and recycling endosomes, respectively (Chavrier et al., 1990; Ullrich et al., 1996). Endosomal trafficking of BMP signaling complexes at the nerve terminals is known to fine-tune the intensity and persistence of BMP signaling (Cosker and Segal, 2014; Deshpande and Rodal, 2016). Altered distribution or misregulation of Rab11 has been shown to suppress Tkv trafficking from early endosome to presynaptic membrane resulting in elevated BMP signaling (O'Connor-Giles et al., 2008; Rodal et al., 2008; Liu et al., 2014; Deshpande and Rodal, 2016).

An important, yet enigmatic question, is the correlation between defective Clathrin-mediated endocytosis (CME) and aberrant synaptic growth. For instance, it is not known whether specific modes of endocytosis externalize specific cargos whose trafficking defect perturbs synaptic signaling. CME, the major endocytic pathway, is required not only for basal synaptic transmission at nerve terminals but also for synapse development (Koh et al., 2004; Dickman et al., 2006; Choudhury et al., 2016). For instance, perturbations in CME resulting from mutations in Dynamin, AP2 subunits, Endo, or Synj all exhibit NMJ structural defects resulting in increased number but decreased size of synaptic boutons in *Drosophila* (Dickman et al., 2006; Choudhury et al., 2016). It is unclear whether the NMJ structural defects associated with the endocytic mutants is a consequence of deficient endosomal trafficking leading to aberrant synaptic signaling. It is likely that perturbing CME deregulates signaling modules of BMP pathway that leads to elevated pMad in the endocytic mutants (O'Connor-Giles et al., 2008; Choudhury et al., 2016).

In central synapses, AP2-dependent CME is dispensable for membrane regeneration from the presynaptic plasma membrane following high-frequency nerve stimulation (Kononenko et al., 2014). However, the critical role of CME in generating vesicles from endosome-like structures following bulk membrane endocytosis cannot be ruled out (Watanabe et al., 2014). Previous studies support a model in which compromised CME can lead to defective signalosome trafficking by trapping signaling molecules in endosomes or intermediate structures of the endosomal pathway (Dubois et al., 2001; Lloyd et al., 2002; Sweeney and Davis, 2002; Wang et al., 2007; Papagiannouli et al., 2019; Joseph et al., 2020). Another study has shown clathrin-independent role of the AP2 in

This work was supported by the Science and Engineering Board (SERB) Project Grant CRG/2021/000599, the Government of India, and by intramural funds from the Indian Institute of Science Education and Research Bhopal (V.K.).

Acknowledgments: We thank Dr. Tsubasa Tanaka for sharing Rab7 and Rab11 antibodies, Dr. Marino Zerial for Rab5 antibodies, and Dr. Peter ten Dijke for pMad antibody. We also thank Dr. Avital Rodal for sharing Rab11 mutants; the Bloomington *Drosophila* Stock Center (BDSC), Vienna *Drosophila* RNAi Centre (VDRC), and *Drosophila* Genomics Resource Centre (DGRC) for fly stocks; Developmental Studies Hybridoma Bank (DSHB), the University of Iowa for monoclonal antibodies; and Dr. Manish Jaiswal for his helpful comments on this manuscript.

*S.D.C. and M.K.D. contributed equally to this work.

S. D. Choudhury's present address: Centralized Core Research Facility, All India Institute of Medical Sciences (AIIMS), Convergence Block, Ansari Nagar, New Delhi 110029, India.

Correspondence should be addressed to Vimlesh Kumar at vimlesh@iiserb.ac.in.

<https://doi.org/10.1523/ENEURO.0044-22.2022>

Copyright © 2022 Choudhury et al.

This is an open-access article distributed under the terms of the Creative Commons Attribution 4.0 International license, which permits unrestricted use, distribution and reproduction in any medium provided that the original work is properly attributed.

the endocytic retrieval of select synaptic vesicle (SV) cargos from the presynaptic cell surface (López-Hernández et al., 2021).

Our previous study has shown elevated levels of synaptic as well as motor-nuclei pMad in $\sigma 2$ -*adaptin* mutants (Choudhury et al., 2016). In order to investigate the underlying signaling mechanisms leading to elevated pMad levels, we performed epistatic interactions between $\sigma 2$ -*adaptin* mutants with the components of BMP signaling. Introducing a mutant copy of *tkv* in $\sigma 2$ -*adaptin* mutants significantly reduces the NMJ overgrowth. Conversely, introducing a mutant copy of inhibitory Smad, *Dad* in a heterozygous $\sigma 2$ -*adaptin* background leads to NMJ overgrowth. Ultrastructural analysis of NMJ revealed accumulation of large vesicles and supports a role of $\sigma 2$ -*adaptin* in generating signalosomes containing vesicles, possibly from endosomal structures. Further analysis of vesicular trafficking using endosomal markers shows that Rab11 is reduced in $\sigma 2$ -*adaptin* mutant NMJ synapses. Thus, our studies reveal a novel function of $\sigma 2$ -*adaptin* in attenuating BMP signaling by facilitating trafficking and recycling of the Tkv receptor.

Materials and Methods

Fly stock

Flies were grown and maintained at 25°C temperature in a standard cornmeal medium as described earlier (Choudhury et al., 2016). Both males and females were used for experiments in the current study. *w*¹¹¹⁸ was used as control unless otherwise stated. Two $\sigma 2$ -*adaptin* alleles were used: *AP2* σ ^{ang7}, which is a hypomorphic allele obtained through a *P*-element mobilization of *Synd*^{EP877} located 2416 bp upstream of the *Syndapin* ORF, and *AP2* σ ^{KG02457}, which is a *P*-element insertion in the third exon of the $\sigma 2$ -*adaptin* ORF making it a null allele (Choudhury et al., 2016). All the mutants, controls, and rescued larvae of either sex were grown under noncrowded conditions on apple agar plates with yeast paste dollop. The following stocks were obtained from Bloomington *Drosophila* Stock Center (BDSC): *tkv*⁷ (BL3242), *Med*¹³ (BL7340), *wit*^{A12} (BL5173), *Dad*^{1E4} (BL10305), *AP2* σ ^{KG02457} (BL13478), *UAS-Rab11-GFP* (BL8506), *Mad*^{k00237} (BL10474), α -*adaptin* dsRNA (BL32866), *Clc* dsRNA (BL27496), *Synj*¹ (BL24883), *Synj*² (BL24884). Other lines used in this study are: *D42-Gal4* (Yeh et al., 1995; Sanyal, 2009), *UAS-tkv-EGFP* (BL51653; Ayyaz et al., 2015), *UAS-YFP-Rab11*^{S25N} (BL9792; Guan et al., 2020), *UAS-Rab11*^{Q70L}-*GFP* (BL23260; Sorvina et al., 2016), *Rab11*^{ex2} and *Rab11*^{93Bi} (Khodosh et al., 2006).

Antibodies and immunocytochemistry

Wandering third instar larvae were dissected in cold calcium-free HL3 saline (70 mM NaCl, 5 mM KCl, 20 mM MgCl₂, 10 mM NaHCO₃, 5 mM Trehalose, 115 mM sucrose, and 5 mM HEPES, pH 7.2) to expose the NMJs and fixed in 4% paraformaldehyde in PBS (pH 7.2) for 30 min at room temperature. Fillets were then washed in PBS containing 0.15% Triton X-100, blocked for 1 h with 5%

bovine serum albumin (BSA), followed by overnight incubation with primary antibody at 4°C. The monoclonal antibody anti-CSP (1:100) was obtained from the Developmental Studies Hybridoma Bank (DSHB). The polyclonal antibody against Rab5 (1:500; Mottola et al., 2010) was a gift from Marino Zerial, Max Planck Institute, Germany. The polyclonal Rab7 (1:500) and Rab11 (1:500; Tanaka and Nakamura, 2008; West et al., 2015) antibodies were a gift from Tsubasa Tanaka, RIKEN Center for Developmental Biology, Japan. The pMad antibody was a gift from Peter ten Dijke and used at 1:1000 dilution (Persson et al., 1998). The secondary antibodies conjugated to Alexa Fluor 488 and Alexa Fluor 568 (Invitrogen, Thermo Fisher Scientific) were used at 1:800 dilution. The Alexa Fluor 488 or Rhodamine-conjugated anti-HRP (Jackson ImmunoResearch) were used at 1:800 dilution. Stained larval fillets were mounted in VECTASHIELD (Vector Laboratories). All the images were captured with a laser scanning confocal microscope (LSM780, Carl Zeiss or FV3000, Olympus Corporation).

Electrophysiology

All intracellular recordings were performed on wandering third instar larvae as described previously (Choudhury et al., 2016). Briefly, HL3 buffer containing 1.5 mM Ca²⁺ was used for larval dissection. Recordings from muscle 6 of A2 hemisegment were performed using sharp glass electrodes having a resistance of 20–25 M Ω . Miniature excitatory junction potentials (mEJPs) were recorded for 60 s, followed by recordings of EJPs at 1 Hz stimulation. For High-frequency recording, nerves were stimulated at 10 Hz, and EJPs were recorded for 5 min. For recording EJPs, stimulation pulse was delivered using Grass S88 stimulator (Grass Instruments, Astro-Med, Inc). The signals were amplified using Axoclamp 900A, digitized using Digidata 1440A, and acquired using pClamp10 software (Molecular Devices). Muscles with resting membrane potential between –60 and –75 mV were used for analysis. The data were analyzed using the Mini Analysis program (Synptosoftware, Decatur).

Intensity profile

Confocal images of muscle four NMJ at A2 hemisegment were used to plot the intensity profile. A single bouton section was used, and the intensities of Tkv and HRP were analyzed by drawing a line across the bouton using Fiji/ImageJ software. The graph was plotted in Microsoft Excel using the intensity values obtained from Fiji/ImageJ software. As the intensity of Tkv in control was too low to plot the graph, all the intensity values were multiplied two-fold.

Electron microscopy

TEM was performed as described previously (Deivasigamani et al., 2015). Briefly, third instar larvae were dissected in cold PBS. The larval fillets were then fixed in 0.12 M cacodylate buffer containing 2% glutaraldehyde for 10 min at room temperature, transferred to a fresh fixative, and kept overnight at 4°C. The fillets

were postfixed for 1 h with 2% osmium tetroxide (OsO_4) solution prepared in 0.12 M cacodylate buffer. The samples were rinsed with 0.12 M cacodylate buffer followed by washes with distilled water to avoid precipitation of cacodylate with Uranyl acetate. Subsequently, the samples were subjected to en bloc staining with 2% uranyl acetate. The stained fillets were again washed with distilled water and dehydrated using graded solutions of ethanol before final infiltration of the samples through propylene oxide for 30 min. Stained and dehydrated fillets were embedded in epoxy resin and hardened overnight at 60°C. Muscles embedded in epoxy resin were sectioned at 60 nm. Ultrathin sections of the muscles stained with 2% uranyl acetate (in 70% ethanol) and 1% aqueous lead citrate were examined at 120 KV on a Tecnai G2 Spirit BioTWIN (FEI) electron microscope. The number of synaptic vesicles per bouton were counted manually using the Multi-point tool in ImageJ/Fiji software and then divided by their respective bouton areas to obtain the vesicle density/ μm^2 area of a bouton. For vesicle size, diameters of at least 100 vesicles from 10 bouton sections of each genotype were used for quantification. For calculating the number of synaptic vesicles docked at the active zones, only those vesicles that were touching the T-bar platform were counted. For calculating the SSR thickness, the scale bar in the images was first calibrated to the number of pixels using the Set scale function in ImageJ/Fiji software. This was followed by using the Straight-line tool to draw a line across the SSR and Measure tool to calculate the thickness.

Western blot analysis

The western blot analysis was done as previously described previously (Choudhury et al., 2016). Briefly, VNC from wandering third instar larvae were dissected out in ice-cold HL3 buffer and homogenized in buffer containing 50 mM Tris-HCl, pH 6.8, 25 mM KCl, 2 mM EDTA, 0.3 M sucrose, and 2% SDS in water. The homogenized sample was then mixed with an equal volume of 2× Laemmli buffer. The protein equivalent to 50 μg was separated on 12% SDS-PAGE and transferred to Hybond-LFP PVDF membrane (GE Healthcare, GE Healthcare Life Sciences). The membrane was then blocked with 5% skimmed milk for 1 h, followed by overnight incubation with anti-Rab11 (1:2000) and anti-Tubulin (1:5000) antibody. IRDye 800 (1:10 000) was used as a secondary antibody, and signals were visualized on LI-COR Odyssey platform. The density of Western bands was quantified using ImageJ/Fiji software.

Quantification and statistical analysis

For fluorescence quantification, images were captured using a laser scanning confocal microscope (LSM780; Carl Zeiss or FV3000, Olympus). All the control and experimental fillets were processed in the same way, and the fluorescence images were captured under the same settings for every experimental set. For bouton quantification, CSP-labeled structures were counted at muscle 6/7 of A2 hemisegment. The number of boutons from each NMJ was normalized to the respective muscle area. To

calculate the bouton number, NMJs from A2 hemisegment were captured using a plan apochromat 40× objective, 1.4 NA and all the CSP positive boutons were counted manually in ImageJ/Fiji software. For muscle area quantification, images from A2 hemisegment were captured using 20× objective, and the area was quantified using ZEN2 software (Carl Zeiss, Germany). For bouton number quantification, the total number of boutons per NMJ was divided by the respective muscle areas. For fluorescence intensity quantification, NMJs from muscle four were captured using a plan apochromat 60×, 1.4 NA objective. For each NMJ, the fluorescence intensity from each bouton was subtracted from the background intensity, and the average intensity was normalized to the control. The fluorescence intensity was calculated using ImageJ/Fiji software. For bouton area quantification, NMJs from muscle 6/7 at A2 hemisegment were captured, and the area was calculated by drawing a free-hand sketch around CSP positive bouton using ImageJ/Fiji software. For multiple comparisons, one-way ANOVA followed by *post hoc* Tukey's test, or Student's *t* test was used. GraphPad Prism 8 was used to plot the graph. Error bars in all the histograms represent SEM. * $p < 0.5$, ** $p < 0.01$, *** $p < 0.001$.

Results

$\sigma 2$ -*adaptin* genetically interacts with regulators of BMP signaling

In a previous study, we showed $\sigma 2$ -*adaptin* mutants caused NMJ overgrowth and upregulation of pMad, an effector of the BMP pathway. Two previously characterized $\sigma 2$ -*adaptin* alleles, $AP2\sigma^{ang7}$, a strong hypomorph and $AP2\sigma^{KG02457}$, a null allele was used in the current study (Choudhury et al., 2016). To explore the role $\sigma 2$ -*adaptin* in regulating BMP signaling at the NMJ, we first assessed the epistatic interaction between $\sigma 2$ -*adaptin* and components of the BMP-signaling pathway. We found that introducing one mutant copy of *tkv*, *Med*, or *Mad* in $\sigma 2$ -*adaptin* mutant background significantly suppressed the synaptic overgrowth phenotype in these animals (Fig. 1A–F). The number of boutons normalized to the muscle area was significantly rescued in $tkv^7/+$; $AP2\sigma^{KG02457}/AP2\sigma^{ang7}$ (1.91 ± 0.12 , $p \leq 0.001$), Med^{13} , $AP2\sigma^{KG02457}/AP2\sigma^{ang7}$ (1.82 ± 0.07 , $p \leq 0.001$), and $Mad^{k00237}/+$; $AP2\sigma^{KG02457}/AP2\sigma^{ang7}$ (2.25 ± 0.11 , $p \leq 0.001$) when compared with $AP2\sigma^{KG02457}/AP2\sigma^{ang7}$ (2.85 ± 0.08 , $p \leq 0.001$). However, there was no significant difference between w^{1118} control, heterozygous $AP2\sigma^{KG02457}/+$, and $tkv^7/+$ (w^{1118} : 1.26 ± 0.06 , $AP2\sigma^{KG02457}/+$: 1.33 ± 0.03 and $tkv^7/+$: 1.34 ± 0.05 ; Fig. 1G).

Consistent with the above observations, we found that mutating one copy of *wit* significantly reduced the $\sigma 2$ -*adaptin* induced synaptic overgrowth (wit^{A12} , $AP2\sigma^{KG02457}/AP2\sigma^{ang7}$: 2.00 ± 0.08 vs $AP2\sigma^{KG02457}/AP2\sigma^{ang7}$: 2.50 ± 0.11 ; $p \leq 0.01$; Extended Data Fig. 1-1). Since elevated BMP signaling results in the formation of smaller boutons, we quantified the bouton area in these genotypes. We found that introducing one copy of tkv^7 ($tkv^7/+$; $AP2\sigma^{KG02457}/AP2\sigma^{ang7}$: 2.9 ± 0.05 , $p \leq 0.01$), Med^{13}

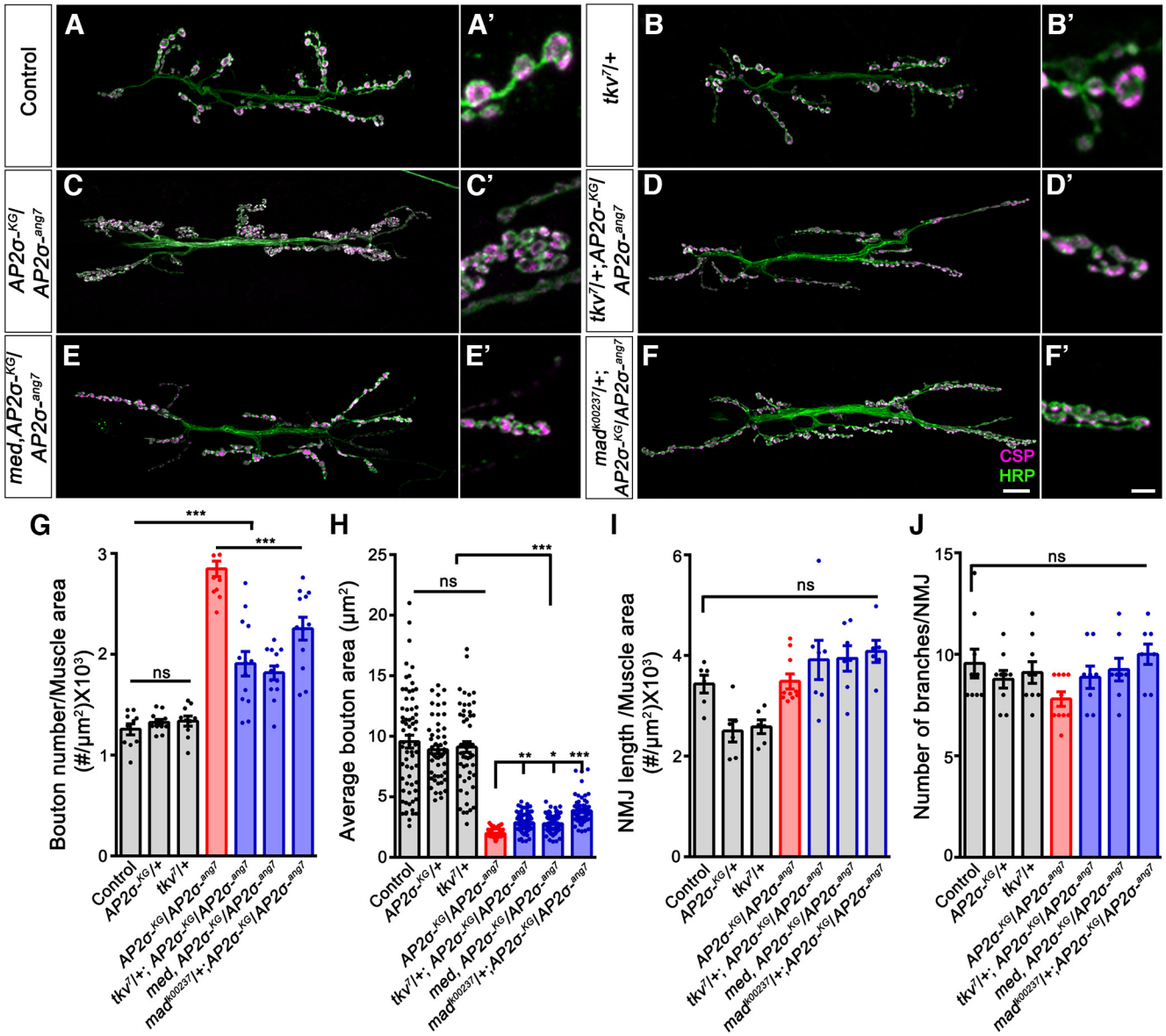


Figure 1. Downregulating BMP signaling components reduced the synaptic overgrowth and clustering in the σ_2 -*adaptin* mutant. **A–F'**, Confocal images of NMJ synapses at muscles 6/7 of A2 hemisegment showing synaptic growth in (**A, A'**) w^{1118} (Control), (**B, B'**) $tkv^7/+$, (**C, C'**) $AP2\sigma^{KG02457}/AP2\sigma^{ang7}$, (**D, D'**) $tkv^7/+; AP2\sigma^{KG02457}/AP2\sigma^{ang7}$, (**E, E'**) $Med^{13}, AP2\sigma^{KG02457}/AP2\sigma^{ang7}$, and (**F, F'**) $Mad^{k00237}/+; AP2\sigma^{KG02457}/AP2\sigma^{ang7}$ double immunolabeled with a presynaptic vesicle marker, CSP (magenta), and a neuronal membrane marker, HRP (green), to mark the bouton outline. Reducing the levels of BMP signaling components in the $AP2\sigma^{KG02457}/AP2\sigma^{ang7}$ background reduces the synaptic overgrowth. Scale bar in **F** (for **A–F**) and **F'** (for **A'–F'**) represents 20 and 5 μm , respectively. **G**, Histogram showing the average bouton number normalized to the muscle area from muscle 6/7 NMJ at A2 hemisegment in control animals (1.26 ± 0.06), $AP2\sigma^{KG02457}/+$ (1.33 ± 0.03), $tkv^7/+$ (1.34 ± 0.05), $AP2\sigma^{KG02457}/AP2\sigma^{ang7}$ (2.85 ± 0.08), $tkv^7/+; AP2\sigma^{KG02457}/AP2\sigma^{ang7}$ (1.91 ± 0.12), $Med^{13}, AP2\sigma^{KG02457}/AP2\sigma^{ang7}$ (1.82 ± 0.07), and $Mad^{k00237}/+; AP2\sigma^{KG02457}/AP2\sigma^{ang7}$ (2.25 ± 0.11). Error bar represents SEM; the statistical analysis was done using one-way ANOVA followed by *post hoc* Tukey's test. **H**, Histogram showing the average bouton area from muscle 6/7 NMJ at A2 hemisegment in control animals (9.57 ± 0.53), $AP2\sigma^{KG02457}/+$ (8.89 ± 0.35), $tkv^7/+$ (9.11 ± 0.46), $AP2\sigma^{KG02457}/AP2\sigma^{ang7}$ (1.98 ± 0.03), $tkv^7/+; AP2\sigma^{KG02457}/AP2\sigma^{ang7}$ (2.85 ± 0.05), $Med^{13}, AP2\sigma^{KG02457}/AP2\sigma^{ang7}$ (2.79 ± 0.05), and $Mad^{k00237}/+; AP2\sigma^{KG02457}/AP2\sigma^{ang7}$ (3.86 ± 0.14). Error bar represents SEM; the statistical analysis was done using one-way ANOVA followed by *post hoc* Tukey's test. * $p < 0.05$, ** $p < 0.01$, *** $p < 0.001$; ns, not significant. **I**, Histogram showing the average NMJ length normalized with muscle area from muscle 6/7 NMJ at A2 hemisegment in control animals (3.43 ± 0.18), $AP2\sigma^{KG02457}/+$ (2.5 ± 0.22), $tkv^7/+$ (2.5 ± 0.14), $AP2\sigma^{KG02457}/AP2\sigma^{ang7}$ (3.49 ± 0.15), $tkv^7/+; AP2\sigma^{KG02457}/AP2\sigma^{ang7}$ (3.91 ± 0.39), $Med^{13}, AP2\sigma^{KG02457}/AP2\sigma^{ang7}$ (3.95 ± 0.25), and $Mad^{k00237}/+; AP2\sigma^{KG02457}/AP2\sigma^{ang7}$ (4.08 ± 0.22). Error bar represents SEM; the statistical analysis was done using one-way ANOVA followed by *post hoc* Tukey's test. ns, not significant. **J**, Histogram showing the average number of branches from muscle 6/7 NMJ at A2 hemisegment in control animals (9.56 ± 0.71), $AP2\sigma^{KG02457}/+$ (8.77 ± 0.43), $tkv^7/+$ (9.11 ± 0.53), $AP2\sigma^{KG02457}/AP2\sigma^{ang7}$ (7.8 ± 0.36), $tkv^7/+; AP2\sigma^{KG02457}/AP2\sigma^{ang7}$ (8.88 ± 0.55), $Med^{13}, AP2\sigma^{KG02457}/AP2\sigma^{ang7}$ (9.25 ± 0.56), and $Mad^{k00237}/+;$

continued

$AP2\sigma^{KG02457}/AP2\sigma^{ang7}$ (10 ± 0.5). Error bar represents SEM; the statistical analysis was done using one-way ANOVA followed by *post hoc* Tukey's test. ns, not significant. Data supporting the rescue of $\sigma2$ -*adaptin* mutant phenotypes by reducing Wnt receptors is shown in Extended Data Figure 1-1.

(Med^{13} , $AP2\sigma^{KG02457}/AP2\sigma^{ang7}$: 2.79 ± 0.05 , $p \leq 0.05$), and $Mad^{k00237}/+$; $AP2\sigma^{KG02457}/AP2\sigma^{ang7}$ (3.86 ± 0.15 , $p \leq 0.001$) in $\sigma2$ -*adaptin* mutant background partially restored the bouton area when compared with $\sigma2$ -*adaptin* mutant alone ($AP2\sigma^{KG02457}/AP2\sigma^{ang7}$: 1.98 ± 0.03 ; w^{1118} controls: 9.5 ± 0.53 ; Fig. 1A'–F',H). Compared with w^{1118} controls, no significant difference was found in the branching and length of the NMJ in these genotypes (Fig. 1I,J). Thus, our data suggest that $\sigma2$ -*adaptin* genetically interacts with the BMP receptors to regulate NMJ bouton number and area.

To further strengthen our observation that $\sigma2$ -*adaptin* attenuates BMP signaling, we tested the interaction between $\sigma2$ -*adaptin* and *Dad*, a negative regulator of BMP signaling (O'Connor-Giles et al., 2008; L Zhao et al., 2013). We first examined the total number of synaptic boutons in transheterozygotes of $\sigma2$ -*adaptin* and *Dad* mutants (Fig. 2). While the number of boutons in larvae heterozygous for $\sigma2$ -*adaptin* [$AP2\sigma^{KG02457}/+$ (1.23 ± 0.05)] and *Dad* [$Dad^{j1E4}/+$ (1.39 ± 0.09)] was comparable with w^{1118} control (1.26 ± 0.06), transheterozygous $Dad^{j1E4}/AP2\sigma^{KG02457}$ (1.89 ± 0.09 , $p \leq 0.001$) showed significantly higher bouton number when compared with w^{1118} controls (Fig. 2H). However, there was no significant difference in the bouton area in transheterozygotes of $\sigma2$ -*adaptin* and *Dad* mutants $Dad^{j1E4}/AP2\sigma^{KG02457}$ (8.51 ± 0.61) when compared with w^{1118} control (10.91 ± 0.87 ; Fig. 2I).

Next, we examined whether neuronally expressing *UAS-Dad* in $\sigma2$ -*adaptin* mutant could rescue the synaptic overgrowth phenotype (Fig. 2E,F). Neuronal expression of *Dad* in $\sigma2$ -*adaptin* mutant background *UAS-Dad/+*; *D42-Gal4*, $AP2\sigma^{ang7}/AP2\sigma^{KG02457}$ (1.87 ± 0.15 , $p \leq 0.001$) significantly rescued the synaptic overgrowth in $\sigma2$ -*adaptin* mutant $AP2\sigma^{ang7}/AP2\sigma^{KG02457}$ (3.1 ± 0.18 , $p \leq 0.001$; Fig. 2G). Moreover, we found that neuronal expression of *Dad* in $\sigma2$ -*adaptin* mutant background partially rescued the average bouton area (*UAS-Dad/+*; *D42-Gal4*, $AP2\sigma^{ang7}/AP2\sigma^{KG02457}$: 5.94 ± 0.29 , $p \leq 0.001$; Fig. 2I). Taken together, these data suggest that $\sigma2$ -*adaptin* regulates BMP signaling to attenuate synaptic growth at the *Drosophila* NMJ.

The functional and morphologic aspects of $\sigma2$ -*adaptin* can be genetically discriminated

Since one mutant copy of BMP receptors in the $\sigma2$ -*adaptin* mutant background significantly restores the morphologic defects, we asked whether the electrophysiological defects associated with the $\sigma2$ -*adaptin* mutant could also be rescued. To address this, we measured evoked excitatory junction potential (EJP), quantal content (QC), and high-frequency intracellular recording on w^{1118} control, heterozygous $tkv^7/+$, $AP2\sigma^{KG02457}/AP2\sigma^{ang7}$, and $tkv^7/+$; $AP2\sigma^{KG02457}/AP2\sigma^{ang7}$ larvae (Fig. 3). We found that

both mEJP amplitude and quantal content in $tkv^7/+$; $AP2\sigma^{KG02457}/AP2\sigma^{ang7}$ (mEJP amplitude = 1.01 ± 0.08 , QC = 38.20 ± 3.09) were not significantly different from $\sigma2$ -*adaptin* mutant $AP2\sigma^{KG02457}/AP2\sigma^{ang7}$ (mEJP = 1.04 ± 0.09 , QC = 39.29 ± 5.81 ; Fig. 3A–D). The scatter plot for mEJP amplitude distribution showed that both $\sigma2$ -*adaptin* mutant and $tkv^7/+$; $AP2\sigma^{KG02457}/AP2\sigma^{ang7}$ had more mEJPs with higher amplitude compared with w^{1118} controls (Fig. 3C). Furthermore, we found that reducing the levels of *Tkv* receptor did not rescue the activity-dependent decline in EJP amplitude. The line plot showed that both $\sigma2$ -*adaptin* mutant and $tkv^7/+$; $AP2\sigma^{KG02457}/AP2\sigma^{ang7}$ followed the same trend of EJP amplitude decline during the high frequency (10 Hz) stimulations (Fig. 3E,F). Moreover, there was no significant difference between w^{1118} and $tkv^7/+$ controls in mEJP amplitude, QC, and high frequency recordings (w^{1118} : mEJP = 0.65 ± 0.03 , QC = 61.92 ± 4.02 ; $tkv^7/+$: mEJP = 0.71 ± 0.05 , QC = 69.77 ± 6.98 ; Fig. 3B,D,F). These data suggest that while reducing BMP signaling by lowering *Tkv* receptors in $\sigma2$ -*adaptin* mutant significantly rescued neuronal overgrowth, it did not restore the physiological deficiencies in $\sigma2$ -*adaptin* mutants indicating that functional and morphologic defects in $\sigma2$ -*adaptin* mutants could be independent of one another.

Loss of $\sigma2$ -*adaptin* leads to the accumulation of endosome-like structures at the NMJ

Studies have shown that internalization and recycling of the membrane and BMP receptors depend on CME and endosomal proteins such as Rab5 and Rab11 (Mitchell et al., 2004; Liu et al., 2014). Mutants with defects in endocytosis and endosomal trafficking cause functional and ultrastructural abnormalities at the synapses. To get a deeper understanding of how loss of $\sigma2$ -*adaptin* affects synapse ultrastructure, we performed transmission electron microscopy on $\sigma2$ -*adaptin* mutant NMJs. Interestingly, ultrastructural analysis of $\sigma2$ -*adaptin* deficient synapses showed an accumulation of large endosome-like structures, similar to what has been shown in mutants that affect endocytic and endosomal recycling machinery such as clathrin (Kasprzewicz et al., 2008; Kawasaki et al., 2011), AP180 (B Zhang et al., 1998), Rab5 (Shimizu et al., 2003), Rab8 (West et al., 2015), and Rab11 (Inoshita et al., 2017). We found decreased synaptic vesicle (SV) density (w^{1118} : 85.18 ± 12.26 vs $AP2\sigma^{KG02457}/AP2\sigma^{ang7}$: 28.02 ± 14 , $p \leq 0.01$) and increased size of the SVs in the $\sigma2$ -*adaptin* mutants (w^{1118} : 43.16 ± 0.94 vs $AP2\sigma^{KG02457}/AP2\sigma^{ang7}$: 71.53 ± 3.70 , $p \leq 0.001$). While there was no change in the number of SVs docked at the active zones (w^{1118} : 0.91 ± 0.20 vs $AP2\sigma^{KG02457}/AP2\sigma^{ang7}$: 0.78 ± 0.28 , $p > 0.05$), we found significantly decreased thickness of the subsynaptic reticulum (SSR; w^{1118} : 0.68 ± 0.03 vs $AP2\sigma^{KG02457}/AP2\sigma^{ang7}$: 0.45 ± 0.03 , $p \leq 0.001$) in the $\sigma2$ -*adaptin* mutants. These ultrastructural

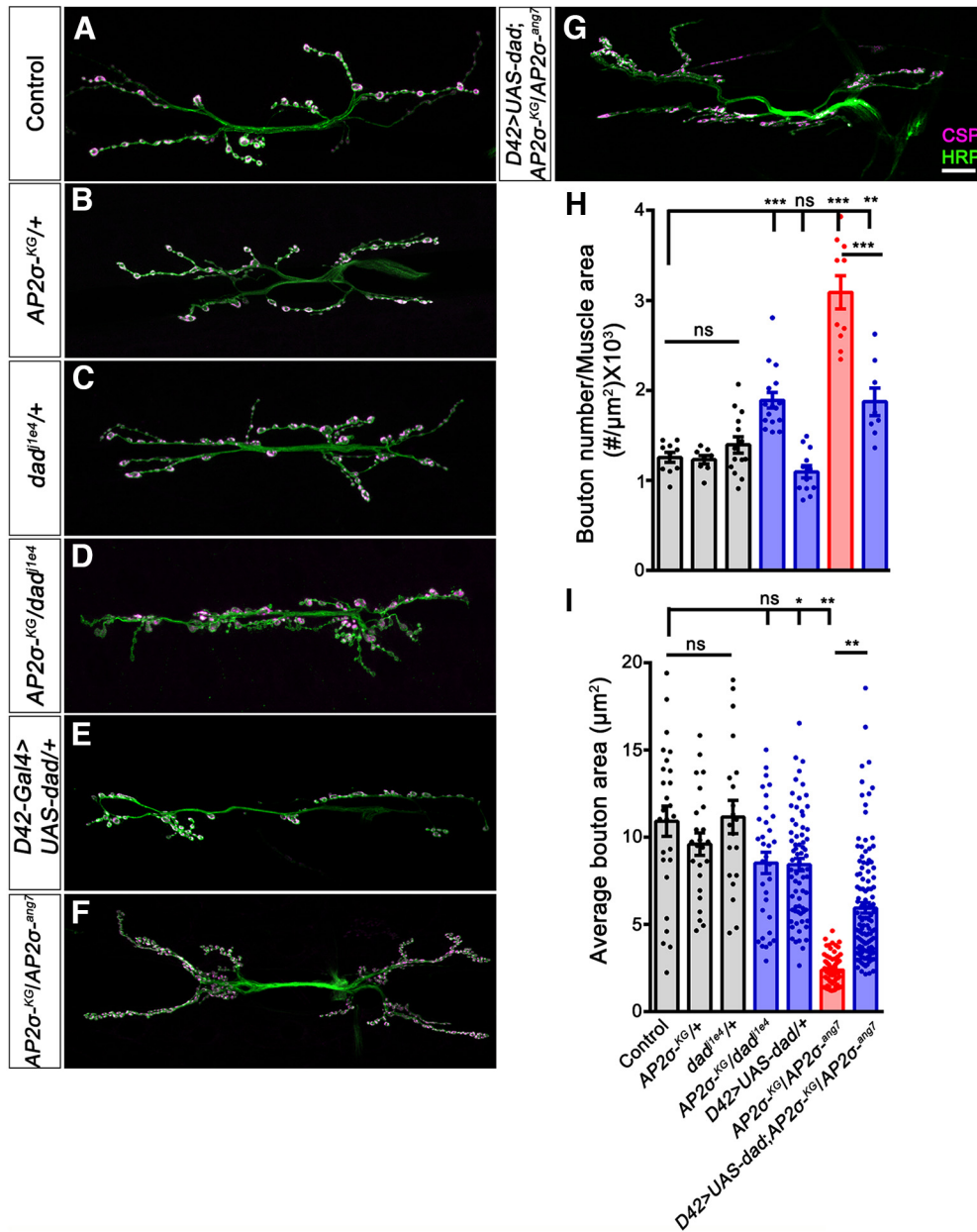


Figure 2. $\sigma 2$ -adaptin genetically interacts with *Dad*, the inhibitory Smad of BMP signaling. **A–G**, Confocal images of NMJ synapses at muscle 6/7 NMJ at A2 hemisegment showing synaptic growth in **(A)** Control, **(B)** $AP2\sigma^{KG02457}/+$, **(C)** $Dad^{j1E4}/+$, **(D)** $AP2\sigma^{KG02457}/Dad^{j1E4}/+$, **(E)** $UAS-Dad/+$; $D42-Gal4/+$, **(F)** $AP2\sigma^{KG02457}/AP2\sigma^{ang7}$, and **(G)** $UAS-Dad/+$; $D42-Gal4$, $AP2\sigma^{ang7}/AP2\sigma^{KG02457}$ double immunolabeled with a presynaptic synaptic vesicle marker, CSP (magenta), and a neuronal membrane marker, HRP (green), to mark the bouton outline. Note that trans-heterozygotes of $\sigma 2$ -adaptin and *Dad* mutants show significantly increased synaptic growth. Scale bar in **G** represents 20 μm . **H**, Histogram showing average bouton number normalized to the muscle area from muscle 6/7 NMJ at A2 hemisegment in control animals (1.26 ± 0.06), $AP2\sigma^{KG02457}/+$ (1.23 ± 0.05), $Dad^{j1E4}/+$ (1.39 ± 0.09), $AP2\sigma^{KG02457}/Dad^{j1E4}/+$ (1.89 ± 0.09), $UAS-Dad/+$; $D42-Gal4/+$ (1.1 ± 0.07), $AP2\sigma^{KG02457}/AP2\sigma^{ang7}$ (3.1 ± 0.18), and $UAS-Dad/+$; $D42-Gal4$, $AP2\sigma^{ang7}/AP2\sigma^{KG02457}$ (1.87 ± 0.15). Error bar represents SEM; statistical analysis was done using one-way ANOVA followed by *post hoc* Tukey’s test. *** $p < 0.001$; ns, not significant. **I**, Histogram showing average bouton area from muscle 6/7 NMJ at A2 hemisegment in control animals (10.91 ± 0.87), $AP2\sigma^{KG02457}/+$ (9.6 ± 0.63), $Dad^{j1E4}/+$ (11.16 ± 0.95), $AP2\sigma^{KG02457}/Dad^{j1E4}/+$ (8.5 ± 0.61), $UAS-Dad/+$; $D42-Gal4/+$ (8.42 ± 0.36), $AP2\sigma^{KG02457}/AP2\sigma^{ang7}$ (2.38 ± 0.11), and $UAS-Dad/+$; $D42-Gal4$, $AP2\sigma^{ang7}/AP2\sigma^{KG02457}$ (5.94 ± 0.3). Error bar represents SEM; statistical analysis was done using one-way ANOVA followed by *post hoc* Tukey’s test. * $p < 0.05$, ** $p < 0.01$; ns, not significant.

defects were rescued on ubiquitous expression of a $\sigma 2$ -adaptin transgene [$actin5C-Gal4/+$; $AP2\sigma^{KG02457}$, $UAS-AP2\sigma/AP2\sigma^{ang7}$: SV density (107.9 ± 11.32), SV size (43.1 ± 1.46), and SSR thickness (0.61 ± 0.01); Fig. 4A–G]. Together,

these data indicate that compromised regeneration of vesicles from the presynaptic membrane and defective membrane recycling in $\sigma 2$ -adaptin mutants results in the accumulation of large endosome-like structures.

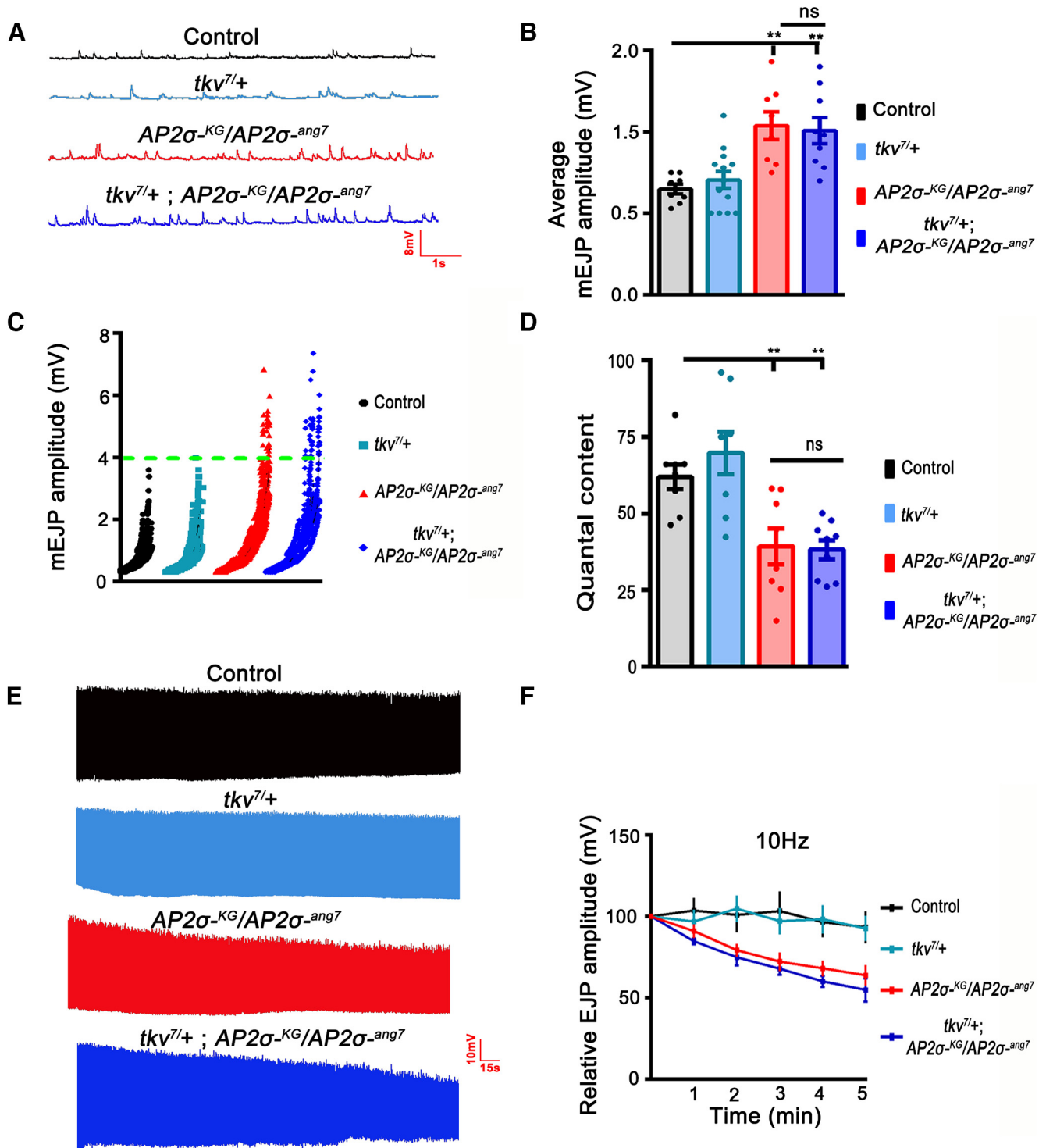


Figure 3. Structural and functional deficits in $\sigma 2$ -adaptin mutant can be genetically discriminated. **A**, Representative traces of mEJP in control, $tkv^{7/+}$, heteroallelic $AP2\sigma^{KG02457}/AP2\sigma^{ang7}$, and $tkv^{7/+}; AP2\sigma^{KG02457}/AP2\sigma^{ang7}$ larvae. **B**, Quantification of average mEJP amplitude in control (0.65 ± 0.03), $tkv^{7/+}$ (0.71 ± 0.05), heteroallelic $AP2\sigma^{KG02457}/AP2\sigma^{ang7}$ (1.04 ± 0.09) and $tkv^{7/+}; AP2\sigma^{KG02457}/AP2\sigma^{ang7}$ (1.01 ± 0.08). At least eight NMJ recordings of each genotype were used for quantification. Error bars represent the SEM; statistical analysis is based on one-way ANOVA followed by *post hoc* Tukey's multiple-comparison test. $**p < 0.01$; ns, not significant. **C**, Scatter plot shows quantification of mEJP amplitude distribution in control, $tkv^{7/+}$, heteroallelic $AP2\sigma^{KG02457}/AP2\sigma^{ang7}$ and $tkv^{7/+}; AP2\sigma^{KG02457}/AP2\sigma^{ang7}$. Note that events with mEJPs greater than 4 mV occurred more frequently in $AP2\sigma^{KG02457}/AP2\sigma^{ang7}$ and $tkv^{7/+}; AP2\sigma^{KG02457}/AP2\sigma^{ang7}$ compared with controls. **D**, Quantification of quantal content in control (61.92 ± 4.02), $tkv^{7/+}$ (69.77 ± 6.98), $AP2\sigma^{KG02457}/AP2\sigma^{ang7}$ (39.29 ± 5.81) and $tkv^{7/+}; AP2\sigma^{KG02457}/AP2\sigma^{ang7}$ (38.2 ± 3.09). At least eight NMJ recordings of each genotype were used for quantification. Error bars represent the SEM; statistical analysis is

continued

based on one-way ANOVA followed by *post hoc* Tukey's multiple-comparison test. $**p < 0.01$; ns, not significant. **E**, Representative traces of EJPs under high-frequency stimulation of control, *tkv*^{+/+}, heteroallelic *AP2* $\sigma^{KG02457}/AP2\sigma^{ang7}$ and *tkv*^{+/+}; *AP2* $\sigma^{KG02457}/AP2\sigma^{ang7}$ larvae stimulated at 10 Hz for 5 min in 1.5 mM Ca²⁺ containing HL3. **F**, Line plot shows quantification of EJP amplitude during 10-Hz high-frequency recordings in control, *tkv*^{+/+}, *AP2* $\sigma^{KG02457}/AP2\sigma^{ang7}$ and *tkv*^{+/+}; *AP2* $\sigma^{KG02457}/AP2\sigma^{ang7}$. Note that the decline in EJP amplitude in $\sigma 2$ -*adaptin* mutant could not be rescued by reducing the levels of Tkv.

$\sigma 2$ -*adaptin* mutants display increased Tkv receptors at the NMJ

AP2 complex has been shown to regulate CME and activity-dependent vesicle regeneration from endosome-like vacuoles (Kononenko et al., 2014; Kadlecova et al., 2017). Since the ultrastructural analysis of $\sigma 2$ -*adaptin* mutants revealed an accumulation of large endosome-like membranous structures similar to mutants with perturbed endocytosis or endosomal trafficking such as *Rab5*, *Rab8*, and *Rab11* mutants (Shimizu et al., 2003; West et al., 2015; Inoshita et al., 2017), we hypothesized that $\sigma 2$ -*adaptin* could be involved either in endocytosis of BMP receptors from the presynaptic membrane or in the endosome-dependent trafficking of the receptors. To test this possibility, we first assessed the level of Tkv receptors at the larval NMJ. Since specific antibodies against Tkv receptors are not available, we expressed an EGFP-tagged Tkv receptor transgene in the motor neurons of $\sigma 2$ -*adaptin* mutants. Interestingly, we found a significant accumulation of Tkv receptors at the mutant synapses (*D42-Gal4, AP2* $\sigma^{KG02457}/AP2\sigma^{ang7}$, *UAS-tkv-EGFP*: 427.5 ± 20.20 , $p \leq 0.001$) when compared with control (*D42-Gal4/UAS-tkv-EGFP*: 100 ± 8.49 ; Fig. 5A–D,I). In order to analyze the subcellular accumulation, we plotted the intensity profiles of Tkv-EGFP and HRP (a presynaptic membrane maker) in single sections of the acquired images. While in control synapses, Tkv localized both at the presynaptic membrane as well as within the bouton; we found a higher intensity peak of Tkv-EGFP at the presynaptic membranes of $\sigma 2$ -*adaptin* mutants (Fig. 5J–O). Consistent with these observations, we found that knocking down α -*adaptin* (*D42-Gal4 > \alpha-adaptin dsRNA*; 276.1 ± 14.75 , $p \leq 0.001$) or clathrin light chain (*Clc*; *D42-Gal4 > Clc dsRNA*; 408.61 ± 21.17 , $p \leq 0.001$) in motor neurons showed significantly increased synaptic Tkv levels (Fig. 5E–I) with intensity profiles similar to that of $\sigma 2$ -*adaptin* mutants (Fig. 5P–U). In contrast, mutants defective in proteins involved in later stages of endocytosis did not show Tkv accumulation at the presynaptic membrane (Fig. 5I), which is consistent with previous studies (O'Connor-Giles et al., 2008; G Zhao et al., 2015). These data indicate that endocytosis/trafficking of Tkv receptors in $\sigma 2$ -*adaptin* mutants is severely compromised, leading to their accumulation at the synaptic membranes.

Loss of $\sigma 2$ -*adaptin* results in decreased levels of recycling endosomal marker Rab11

Receptors are known to be endocytosed, trafficked to early endosomes, and sorted out for recycling back to the membrane or degraded in the lysosomes (Dunn et al., 1989; Gruenberg et al., 1989; Jovic et al., 2010). This process is mediated by the Rab family of small GTPases

(Schwartz et al., 2007). Since the ultrastructural analysis of $\sigma 2$ -*adaptin* mutant synapse showed an accumulation of enlarged synaptic vesicles similar to mutants of the endolysosomal pathway (Shimizu et al., 2003; West et al., 2015; Inoshita et al., 2017), we next asked whether this pathway has any role in the accumulation of Tkv in $\sigma 2$ -*adaptin* mutants. We found that the synaptic levels of the early endosomal marker, Rab5 (w^{1118} : 100.0 ± 3.0 vs *AP2* $\sigma^{KG02457}/AP2\sigma^{ang7}$: 97.25 ± 4.81) or the late endosomal marker, Rab7 (w^{1118} : 100.0 ± 5.71 vs *AP2* $\sigma^{KG02457}/AP2\sigma^{ang7}$: 115.6 ± 8.17) were not altered in $\sigma 2$ -*adaptin* mutant synapses (Fig. 6A–J). However, we observed reduced synaptic Rab11 levels (w^{1118} : 100.0 ± 5.73 vs *AP2* $\sigma^{KG02457}/AP2\sigma^{ang7}$: 61.81 ± 7.10 , $p \leq 0.001$) in $\sigma 2$ -*adaptin* mutant synapses (Fig. 6K–S). Western blot analysis revealed that total levels of Rab11 protein in $\sigma 2$ -*adaptin* mutants were not altered compared with w^{1118} controls (Extended Data Fig. 6-1). Synaptic Rab11 levels were restored to w^{1118} control levels on neuronal expression of a $\sigma 2$ -*adaptin* transgene in the $\sigma 2$ -*adaptin* mutant (*D42-Gal4, AP2* $\sigma^{KG02457}/UAS-AP2\sigma$, *AP2* σ^{ang7} : 112.9 ± 8.29 ; Figure 6O,P,S). Taken together, these data indicate that: (1) compromised endocytosis, and possible defective recycling of the endocytosed Tkv receptors result in their accumulation at the synapse, or/and (2) AP2 complex may regulate Tkv sorting possibly through the endosomal pathway.

Rab11 mutants phenocopy BMP-signaling and NMJ defects of $\sigma 2$ -*adaptin*

Rab11 has been shown to regulate BMP signaling at the *Drosophila* NMJ (Khodosh et al., 2006; Liu et al., 2014). Because $\sigma 2$ -*adaptin* mutant synapses showed reduced Rab11 levels, we next asked whether Rab11 had a role in regulating Tkv receptor trafficking. We first examined the levels of pMad and Tkv in *Rab11* mutants. We found that *Rab11* mutants, as well as animals expressing a dominant-negative form of Rab11 in motor neurons, showed accumulation of pMad at the NMJ synapses (w^{1118} : 100 ± 5.87 ; *Rab11*^{ex2/93Bi}: 147.9 ± 8.58 , $p \leq 0.01$; *UAS-YFP-Rab11*^{S25N}/+; *D42-Gal4*/+; 134.2 ± 4.36 , $p \leq 0.05$; *AP2* $\sigma^{KG02457}/AP2\sigma^{ang7}$: 218.8 ± 7.5 , $p \leq 0.001$; Fig. 7A–H,M). We further assessed Tkv receptor levels in these mutant synapses and found that *Rab11* mutants also showed increased Tkv levels at the synapse (*D42-Gal4, Rab11*^{ex2/93Bi}/+; *tkv-EGFP*, *Rab11*^{93Bi}: 189.5 ± 10.57) compared with control animals (*D42-Gal4/tkv-EGFP*: 100 ± 8.71). However, the Tkv enrichment pattern was not the same as that in $\sigma 2$ -*adaptin* mutants (Fig. 7I–L,N). While $\sigma 2$ -*adaptin* mutants showed Tkv enrichment at the synaptic membranes, *Rab11* mutants had punctate Tkv localization within the boutons, but showed no enrichment at the presynaptic

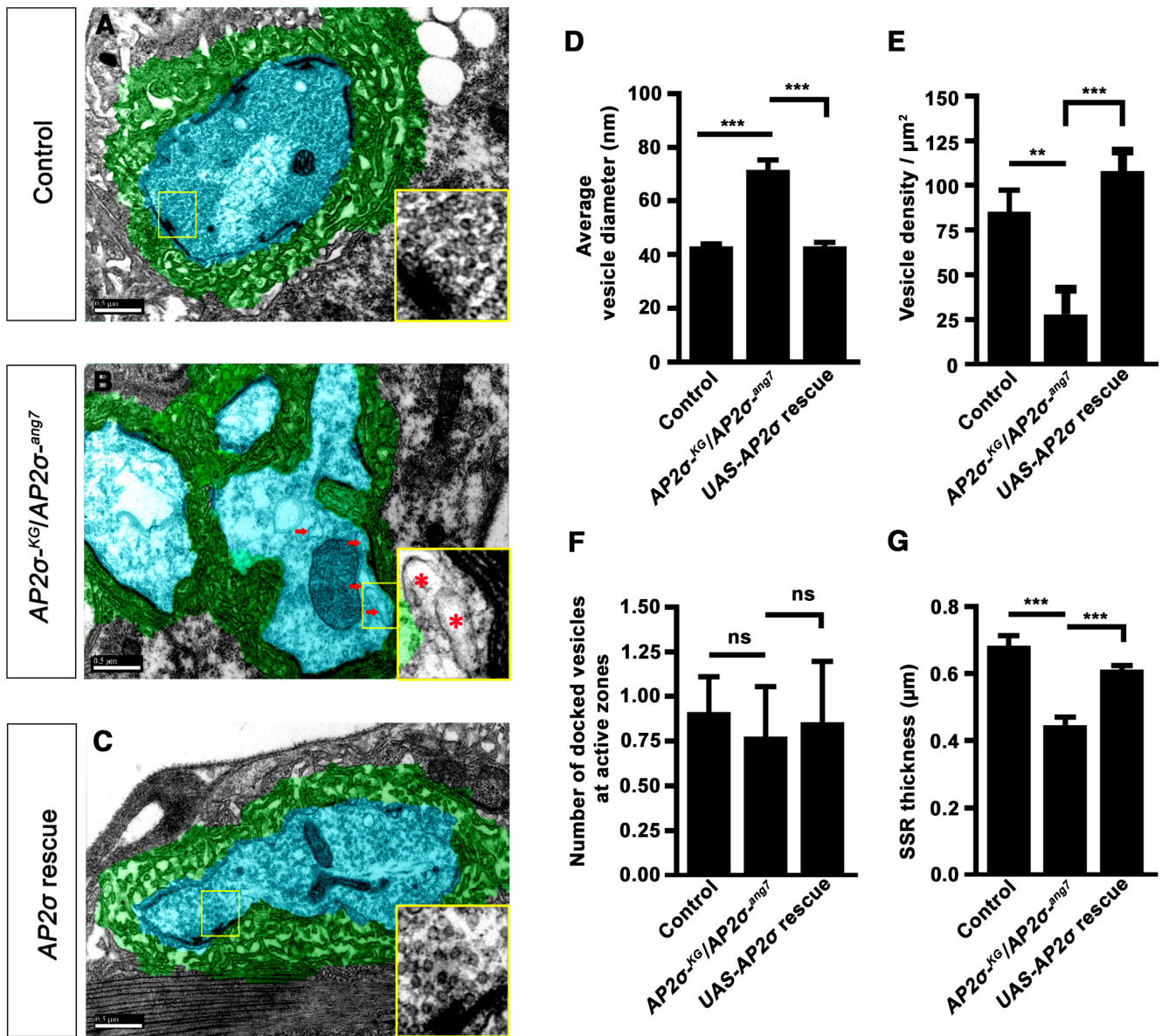


Figure 4. $\sigma 2$ -adaptin mutant synapses show accumulation of large endosome-like vesicular structure. **A–C**, Electron micrographs of third instar Type Ib boutons of control (**A**), $AP2\sigma^{KG02457}/AP2\sigma^{ang7}$ (**B**), and $actin5C/+; AP2\sigma^{KG02457}, UAS-AP2\sigma/AP2\sigma^{ang7}$ (**C**). Arrows point to the large endosome-like vesicular structures observed in $AP2\sigma^{KG02457}/AP2\sigma^{ang7}$ boutons but are absent in control and rescued boutons. The insets show a magnified area around the active zones. The presynaptic compartment is pseudocolored in cyan, and the subsynaptic reticulum is marked in green. Scale bar represents 500 nm. **D**, Histogram showing average vesicle diameter in control (43.16 ± 0.94), $AP2\sigma^{KG02457}/AP2\sigma^{ang7}$ (71.53 ± 3.7), and $actin5C/+; AP2\sigma^{KG02457}, UAS-AP2\sigma/AP2\sigma^{ang7}$ (43.1 ± 1.46). Error bar represents SEM; statistical analysis was done using one-way ANOVA followed by *post hoc* Tukey's test. $***p < 0.001$, $**p < 0.01$. **E**, Histogram showing SV density per unit area in control (85.18 ± 12.26), $AP2\sigma^{KG02457}/AP2\sigma^{ang7}$ (28.02 ± 14), and $actin5C/+; AP2\sigma^{KG02457}, UAS-AP2\sigma/AP2\sigma^{ang7}$ (107.9 ± 11.32). At least 10 images from three different larvae per genotype were used for quantification. Error bar represents SEM; statistical analysis was done using one-way ANOVA followed by *post hoc* Tukey's test. $***p < 0.001$, $**p < 0.01$. **F**, Histogram showing average number of synaptic vesicles docked at the active zones in control (0.91 ± 0.20), $AP2\sigma^{KG02457}/AP2\sigma^{ang7}$ (0.78 ± 0.28), and $actin5C/+; AP2\sigma^{KG02457}, UAS-AP2\sigma/AP2\sigma^{ang7}$ (0.86 ± 0.34). At least five images from three different larvae per genotype were used for quantification. Error bar represents SEM; statistical analysis was done using one-way ANOVA followed by *post hoc* Tukey's test. ns, not significant. **G**, Histogram showing SSR thickness in control (0.68 ± 0.03), $AP2\sigma^{KG02457}/AP2\sigma^{ang7}$ (0.45 ± 0.03), and $actin5C/+; AP2\sigma^{KG02457}, UAS-AP2\sigma/AP2\sigma^{ang7}$ (0.61 ± 0.01). At least five images from three different larvae per genotype were used for quantification. Error bar represents SEM; statistical analysis was done using one-way ANOVA followed by *post hoc* Tukey's test. $***p < 0.001$.

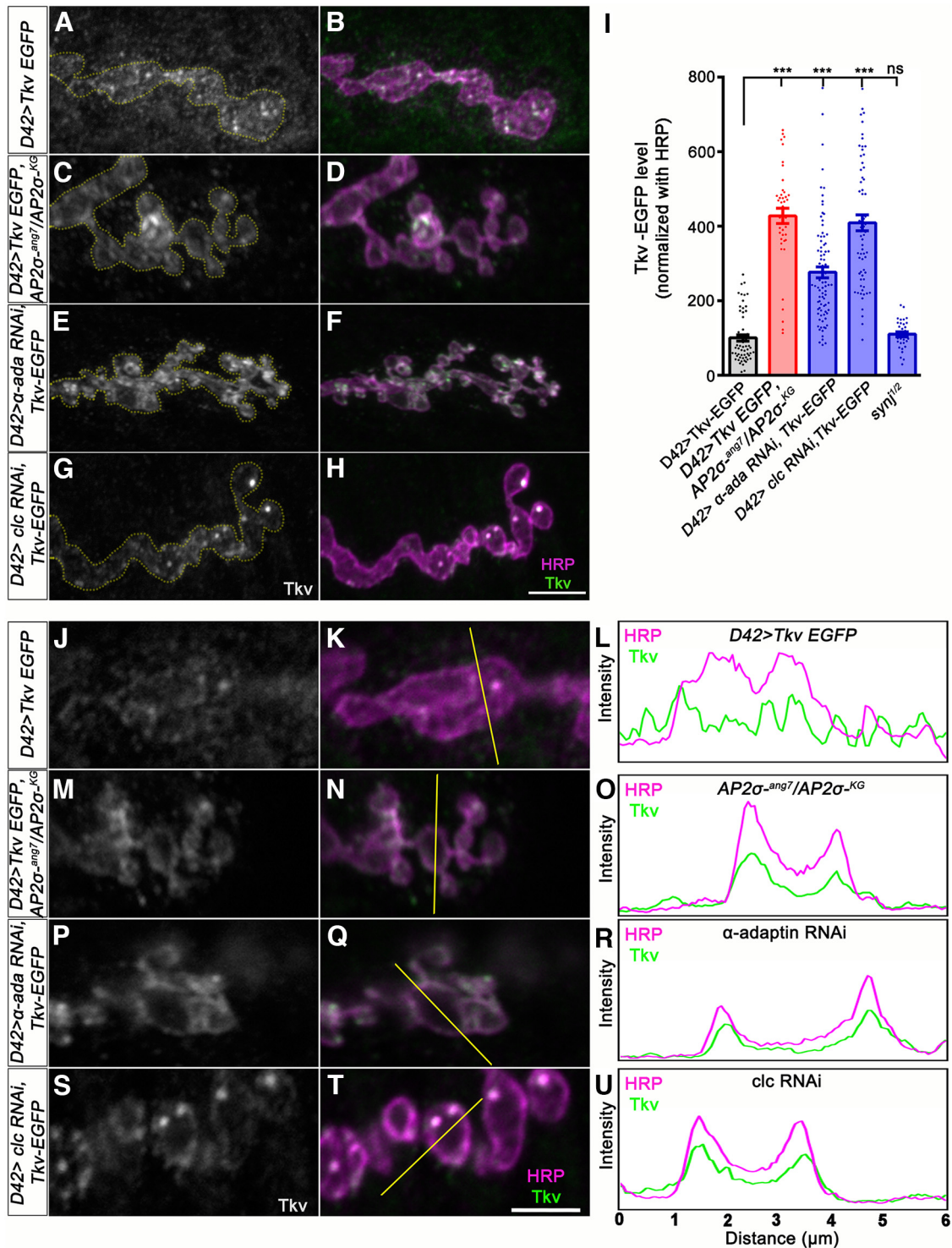


Figure 5. Neuronal reduction of subunits of AP2 complex or clathrin leads to accumulation of synaptic Tkv. **A–H**, Confocal images of NMJ synapses at muscle 4 NMJ at A2 hemisegment in control, *D42-Gal4/UAS-tkv-EGFP* (**A, B**), *D42-Gal4, AP2σ^{KG02457}/AP2σ^{ang7}, UAS-tkv-EGFP* (**C, D**), *D42-Gal4, tkv-EGFP/α-adaptin dsRNA* (**E, F**), and *D42-Gal4, tkv-EGFP/Clc dsRNA* (**G, H**). The neuronal membrane is marked with HRP (magenta), and EGFP fluorescence is shown in grayscale/green. The bouton area is outlined in the gray channel. Scale bar in **H** represents 5 μm. **I**, Histogram showing the relative Tkv level normalized to HRP in *D42-Gal4/UAS-tkv-EGFP* (100 ± 8.489), *D42-Gal4, AP2σ^{KG02457}/AP2σ^{ang7}, UAS-tkv-EGFP* (427.5 ± 20.2), *D42-Gal4, tkv-EGFP/α-adaptin dsRNA* (276.1 ± 14.75), *D42-Gal4, tkv-EGFP/Clc dsRNA* (408.6 ± 21.17), and *Synj^{1/2}* (110.1 ± 6.65) synapses. Error bars represent SEM; statistical analysis is based on one-way ANOVA followed by *post hoc* Tukey’s multiple-comparison test. ****p* < 0.001; ns, not significant. **J–U**, A single confocal section of a bouton labeled for Tkv (represented in grayscale) and presynaptic membrane marker HRP (magenta) in *D42-Gal4/UAS-tkv-EGFP* (**J, K**) or *D42-Gal4, AP2σ^{KG02457}/AP2σ^{ang7}, UAS-tkv-EGFP* (**M, N**), *D42-Gal4, tkv-EGFP/α-adaptin dsRNA* (**P, Q**), and *D42-Gal4, tkv-EGFP/Clc dsRNA* (**S, T**). **L–U**, Line graphs showing the intensity profiles of HRP (magenta) and Tkv (green) across the bouton area in the corresponding genotypes.

continued

$\sigma 2$ -*adaptin* dsRNA (**P, Q**), and *D42-Gal4, tkv-EGFP/Clc* dsRNA (**S, T**). Note that the intensity profile plot across bouton (shown in **L, O, R, U** as a thin line) shows that $\sigma 2$ -*adaptin* mutant (**O**), *D42-Gal4*> $\sigma 2$ -*adaptin* dsRNA (**R**), and *D42-Gal4*>*Clc* dsRNA (**U**) has more Tkv receptors at the membrane compared with control (**L**). Scale bar in **T** represents 2.5 μm .

membrane (Extended Data Fig. 7-1). This suggests that while Rab11 does not affect the internalization of Tkv, a defective vesicular trafficking pathway in *Rab11* mutants probably leads to the enrichment of Tkv receptors in endosome-like compartments.

Since $\sigma 2$ -*adaptin* mutants showed reduced Rab11 levels at the NMJ, we next asked whether Rab11 was responsible for the morphologic defects in these mutants. To assess this, we first examined whether reducing Rab11 levels phenocopied $\sigma 2$ -*adaptin* mutations. Interestingly, we found that *Rab11* mutants or neuronal expression of a dominant-negative form of Rab11 (*Rab11*^{S25N}) indeed phenocopied the NMJ morphologic defects in $\sigma 2$ -*adaptin* mutants and showed NMJ overgrowth (*w*¹¹¹⁸: 1.56 ± 0.06 ; *Rab11*^{ex2/93 Bi}: 2.77 ± 0.11 , $p \leq 0.001$; *UAS-YFP-Rab11*^{S25N/+}; *D42-Gal4/+*: 2.26 ± 0.08 , $p \leq 0.001$; and *AP2* σ ^{KG02457/AP2 σ ^{ang7}: 2.83 ± 0.12 , $p \leq 0.001$; Fig. 8A–F). Expressing a wild-type or constitutively active form of Rab11, however, did not alter the synaptic morphology (Extended Data Fig. 8-1). We next examined whether neuronal expression of Rab11 could restore the synaptic overgrowth in $\sigma 2$ -*adaptin* mutants. We found that expressing the wild-type form of Rab11 in $\sigma 2$ -*adaptin* mutant background (*UAS-YFP-Rab11*^{WT/+}; *D42-Gal4, AP2* σ ^{ang7/AP2 σ ^{KG02457}: 2.83 ± 0.16 , ns) did not prevent the synaptic overgrowth (Fig. 8E,F). Moreover, expressing a constitutively active form of Rab11 (*Rab11*^{CA}; *UAS-YFP-Rab11*^{CA/+}; *D42-Gal4, AP2* σ ^{ang7/AP2 σ ^{KG02457}: 2.5 ± 0.14 , ns) failed to prevent the synaptic overgrowth in $\sigma 2$ -*adaptin* mutants (Extended Data Fig. 8-2). Consistent with this, expression of *Rab11*^{WT}, *Rab11*^{DN}, or *Rab11*^{CA} in $\sigma 2$ -*adaptin* mutant background did not rescue the functional defects in $\sigma 2$ -*adaptin* mutant (Extended Data Figs. 8-3, 8-4). Taken together, these results suggest that $\sigma 2$ -*adaptin* is crucial for the proper localization of Rab11 at the synapses and possibly required for the formation of the Rab11 positive recycling endosomes. We surmise that these recycling endosomes could be essential for targeting and distributing Tkv receptors at the synapses to regulate BMP signaling.}}}

In conclusion, $\sigma 2$ -*adaptin* and *Rab11* increase Tkv accumulation and BMP signaling to generate similar NMJ phenotypes via independent pathways.

Discussion

Compromised endocytosis not only perturbs synaptic transmission but also has been implicated in deregulating synaptic growth as demonstrated in *Endo*, *Synj*, *nwk*, *shi*, *Clc*, *brat*, and $\sigma 2$ -*adaptin* mutant NMJs (Rikhy et al., 2002; Verstreken et al., 2002; Verstreken et al., 2003; Choudhury et al., 2016). The underlying molecular mechanism by which these proteins regulate synaptic growth, however, has only been demonstrated for *nwk* and *brat* (O'Connor-Giles et al., 2008; Shi et al., 2013). Our previous study on $\sigma 2$ -*adaptin* mutants showed no change in

levels of endocytic proteins like *Endo*, *Synj*, and *Dyn* (Choudhury et al., 2016), prompting us to investigate the role of $\sigma 2$ -*adaptin* in synaptic growth signaling. Mutations that affect endocytosis, in general, show synaptic overgrowth and increased BMP effector, pMad. The signaling output of growth-regulating pathways is often dependent on intracellular traffic that in part is dependent on endocytosis of activated receptors, ultimately impinging on the BMP, JNK, or Wingless pathways (Shi et al., 2013; Deshpande and Rodal, 2016). Here, we show for the first time that $\sigma 2$ -*adaptin* genetically interacts with BMP signaling pathway at the synapse. Loss of $\sigma 2$ -*adaptin* leads to accumulation of Tkv receptor at the NMJ. Additionally, we provide evidence that $\sigma 2$ -*adaptin* regulates the localization of recycling endosomal protein Rab11.

$\sigma 2$ -*adaptin* genetically interacts with BMP pathway to regulate neuronal BMP signaling

Endosomal trafficking of BMP receptors is a crucial regulatory mechanism that controls synaptic growth (Rodal et al., 2011). Various proteins interact with BMP receptors to facilitate or attenuate the BMP-dependent signaling cascade (McCabe et al., 2004; XW Zhang et al., 2017). Endocytic proteins appear to be fascinating candidates as BMP receptor interactors. *Drosophila* loss-of-function endocytic mutants correlate with elevated BMP signaling and neuronal overgrowth phenotype (Dickman et al., 2006; Rodal et al., 2011; Deshpande and Rodal, 2016). Consistent with this, we show that increased Tkv levels at the NMJ result in elevated BMP signaling in $\sigma 2$ -*adaptin* mutants. If the BMP pathway is responsible for the synaptic overgrowth in $\sigma 2$ -*adaptin* mutants, we reasoned that reducing the levels of BMP signaling components should rescue the NMJ phenotype. In agreement with this, we found that partially reducing BMP receptors Tkv, Wit, and cytosolic co-Smad molecule, Medea, significantly rescues the NMJ defects in $\sigma 2$ -*adaptin* mutants. Our data reveal that $\sigma 2$ -*adaptin* genetically interacts with the negative regulator of BMP signaling, the inhibitory Smad, Dad. Transheterozygotes of *Dad* and $\sigma 2$ -*adaptin* mutants have increased number of boutons compared with heterozygotes of either mutant alone. Consistent with this inference, neuronal expression of *UAS-Dad* in $\sigma 2$ -*adaptin* mutant background significantly reduces the synaptic overgrowth phenotype. However, reducing BMP signaling only partially reduces the bouton size in $\sigma 2$ -*adaptin* mutants. There could be at least two plausible explanations for the partial rescue of the bouton size: first, removing only one copy of *tkv* may not be sufficient for rescuing this defect. Since mutating both copies of *tkv* results in embryonic lethality, we could not test the epistatic interactions by removing both the copies of Tkv in $\sigma 2$ -*adaptin* mutants. Second, $\sigma 2$ -*adaptin* may regulate NMJ bouton size through a different signaling pathway, which

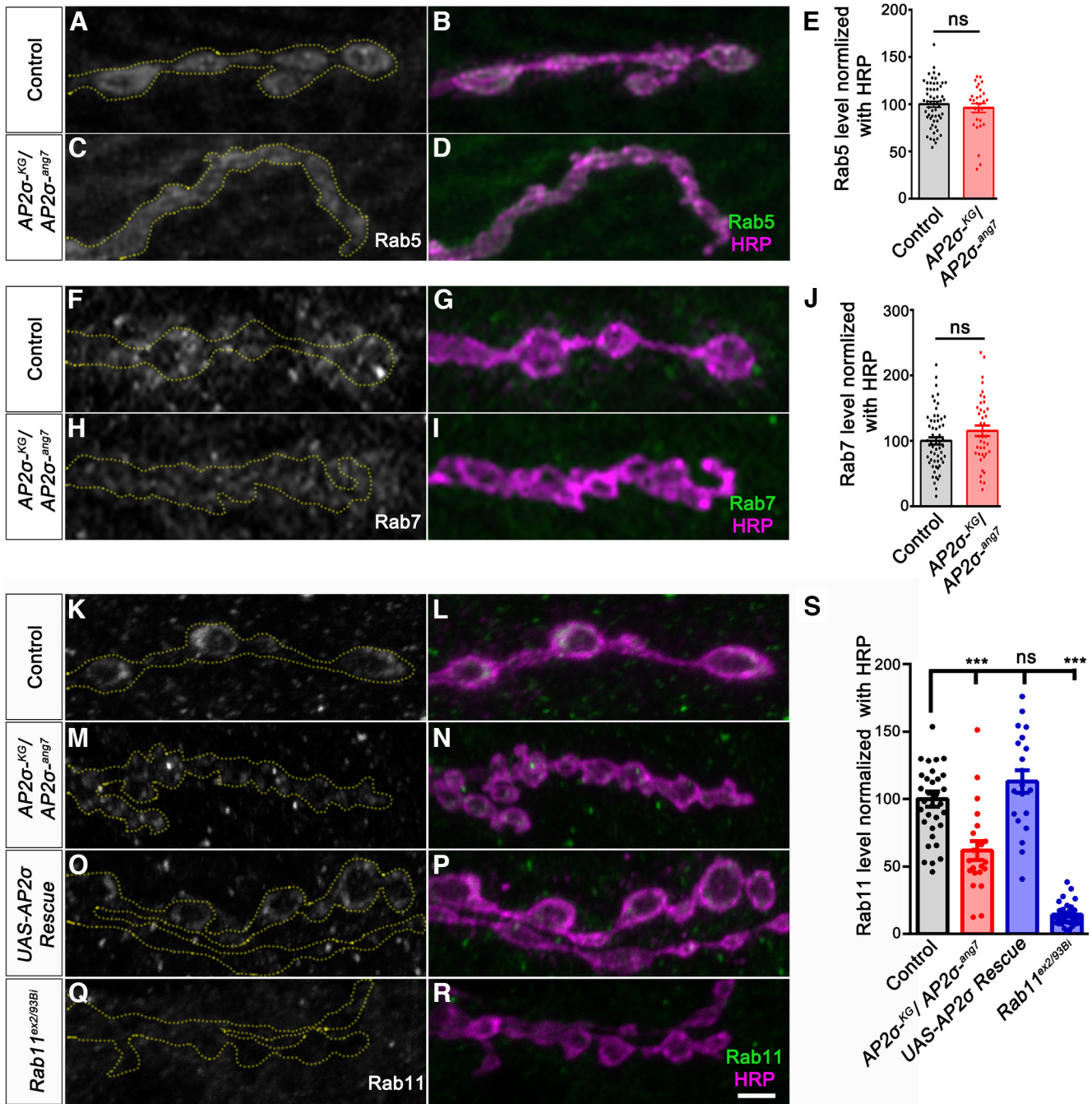


Figure 6. $\sigma 2$ -adaptin mutant synapses show a reduction in the recycling endosome marker, Rab11. **A–D**, Confocal images of NMJ synapses at muscle 4 of A2 hemisegment in control (**A, B**), $AP2\sigma^{KG02457}/AP2\sigma^{ang7}$ (**C, D**), double immunolabeled with early endosomal marker Rab5 (represented in grayscale/green) and neuronal membrane marker, HRP (magenta). **E**, Histogram showing the Rab5 level in control (100.0 ± 3.0) and $AP2\sigma^{KG02457}/AP2\sigma^{ang7}$ (97.25 ± 4.81) synapse. Error bar represents SEM; statistical analysis was done using Student’s *t* test. ns, not significant. **F–I**, Confocal images of NMJ synapses at muscle 4 of A2 hemisegment in control (**F, G**), $AP2\sigma^{KG02457}/AP2\sigma^{ang7}$ (**H, I**), double immunolabeled with late endosomal marker, Rab7 (represented in grayscale/green), and neuronal membrane marker, HRP (magenta). **J**, Histogram showing the Rab7 level in control (100.0 ± 5.71) and $AP2\sigma^{KG02457}/AP2\sigma^{ang7}$ (115.6 ± 8.17) synapse. Error bar represents SEM; statistical analysis was done using Student’s *t* test. ns, not significant. **K–R**, Confocal images of NMJ synapses at muscle 4 of A2 hemisegment in control (**K, L**), $AP2\sigma^{KG02457}/AP2\sigma^{ang7}$ (**M, N**), $D42-Gal4, AP2\sigma^{KG02457}/UAS-AP2\sigma, AP2\sigma^{ang7}$ (**O, P**), and $Rab11^{ex2/93Bi}$ (**Q, R**) double immunolabeled with recycling endosomal marker, Rab11 (represented in grayscale/green), and neuronal membrane marker, HRP (magenta). Scale bar in **R** represents 3 μ m. **S**, Histogram showing relative Rab11 level normalized to HRP in control (100 ± 5.73), $AP2\sigma^{KG02457}/AP2\sigma^{ang7}$ (61.81 ± 7.11); $D42-Gal4, AP2\sigma^{KG02457}/UAS-AP2\sigma, AP2\sigma^{ang7}$ (112.9 ± 8.29) and $Rab11^{ex2/93Bi}$ (14.21 ± 1.57) synapses. Error bars represent SEM; statistical analysis is based on one-way ANOVA followed by *post hoc* Tukey’s multiple-comparison test. ****p* < 0.001; ns, not significant. The data supporting that the levels of Rab11 is not altered in $\sigma 2$ -adaptin mutants is provided in Extended Data Figure 6-1.

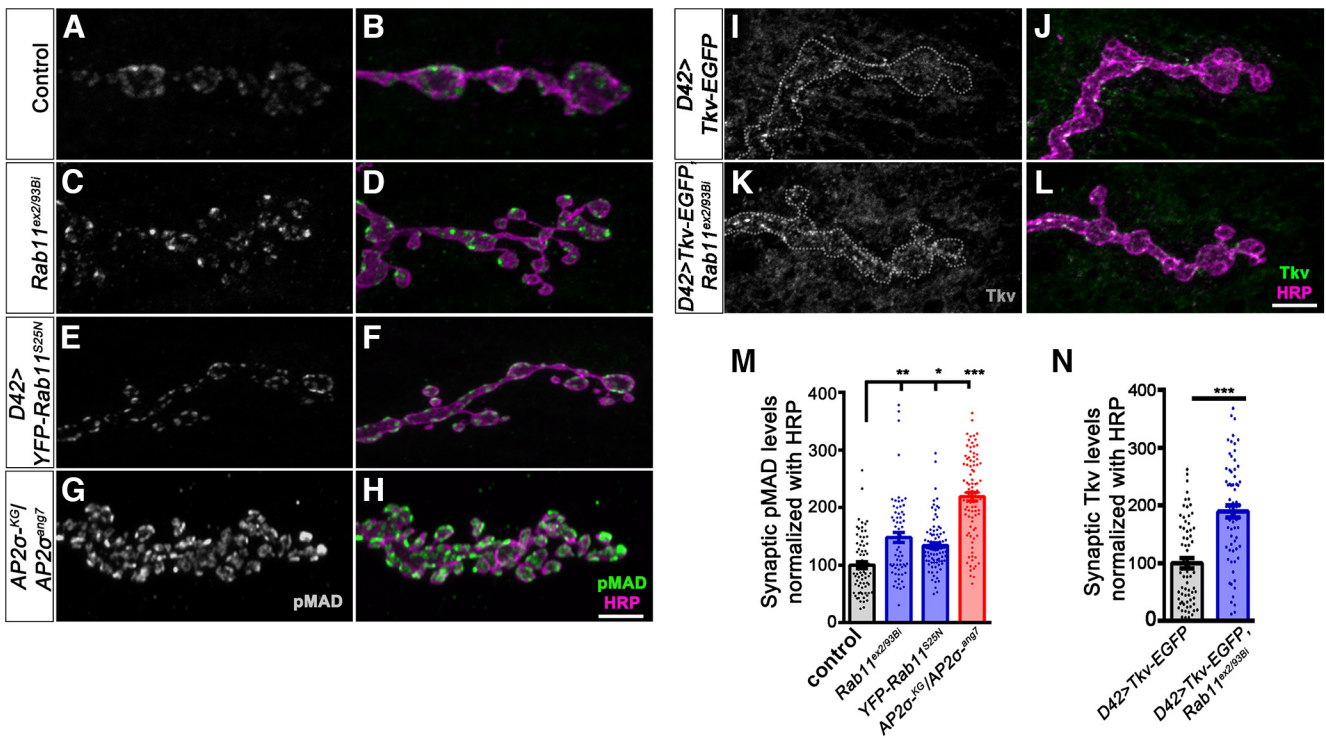


Figure 7. Rab11 mutants show elevated levels of synaptic pMad and Tkv. **A–H**, Confocal images of NMJ from muscle 4 at A2 hemisegment in control (**A, B**), *Rab11^{ex2/93 Bi}* (**C, D**), *D42-Gal4*-driven dominant-negative *YFP-Rab11^{S25N}* (**E, F**), and *AP2σ^{KG02457}/AP2σ^{ang7}* (**G, H**) double immunolabeled with pMad (grayscale/green) and a neuronal membrane marker, HRP (magenta) to mark the bouton outline. Scale bar in **H** represents 5 μm. **I–L**, Confocal images of NMJ from muscle 4 at A2 hemisegment in *D42-Gal4*-driven *tkv-EGFP* (**I, J**) and *D42-Gal4*-driven *tkv-EGFP, Rab11^{ex2}/Rab11^{93Bi}* (**K, L**) double immunolabeled with Tkv (grayscale/green) and a neuronal membrane marker, HRP (magenta) to mark the bouton outline. Scale bar in **L** represents 5 μm. **M**, Histogram showing the levels of pMad normalized with HRP from muscle 4 at A2 hemisegment in control (100 ± 5.87), *Rab11^{ex2/93 Bi}* (147.9 ± 5.88), *D42*-driven *YFP-Rab11^{S25N}* (134.2 ± 4.36), and *AP2σ^{KG02457}/AP2σ^{ang7}* (218.8 ± 7.5). The error bar represents SEM; statistical analysis was done using one-way ANOVA followed by *post hoc* Tukey’s test. ****p* < 0.001, ***p* < 0.01, **p* < 0.05. **N**, Histogram showing the relative Tkv level normalized to HRP in *D42-Gal4*-driven *tkv-EGFP* (100 ± 8.71), and *D42-Gal4, Rab11^{ex2}/tkv-EGFP, Rab11^{93Bi}* (189.5 ± 10.57). Error bar represents SEM; statistical analysis was done using Student’s *t* test. ****p* < 0.001. The data supporting that the Tkv receptor is not enriched at the presynaptic membrane in *Rab11* mutants is shown in Extended Data Figure 7-1.

remains to be elucidated. Overall, our data suggest that σ 2-adaptin negatively regulates the BMP growth signaling pathway to attenuate synaptic growth.

σ 2-adaptin regulates trafficking of Thickveins at the NMJ

BMP signaling has been extensively studied in the context of neuronal growth in which the activated Tkv is endocytosed and fuse with the early endosomes, where it activates downstream signaling molecules. The signaling is attenuated when these activated receptor-containing vesicles recycle back to the plasma membrane or fuse with lysosomes for degradation (Rodal et al., 2011; Smith et al., 2012). Trafficking of these receptors into and out of such endosomes provides an additional tier for spatial and temporal modulation of signal transduction. The members of the Rab family of small GTPases regulate various stages of endocytosis (Kelly et al., 2012). Our immunocytochemistry data show elevated Tkv receptor levels at the synapses and motor neuron soma (data not shown) of σ 2-adaptin mutants. Besides, levels of Rab11

(known for its role in the recycling of Tkv receptor) are reduced by half in σ 2-adaptin mutant synapses.

Interestingly, levels of early and late endosomes marked with Rab5 and Rab7, respectively, remain unaffected at the σ 2-adaptin mutant synapses. The intensity profile of Tkv and HRP across the bouton shows that σ 2-adaptin mutant has a higher intensity of Tkv at the membrane, indicating that a significant proportion of the Tkv receptors are accumulated at the presynaptic membrane. The pattern of Tkv enrichment in σ 2-adaptin and *Rab11* mutants were distinct. While σ 2-adaptin mutant synapses showed Tkv enriched at synaptic membranes, *Rab11* mutants had a rather punctate distribution within the bouton. The differential distribution of these proteins could be because of their distinct roles in the neurons. While σ 2-adaptin plays a critical role in retrieving the SV-membrane from the presynaptic membrane, Rab11 is a component of the endolysosomal machinery. A clear separation of Tkv signals/pixels distinguishing plasma membrane Tkv from endosomal Tkv is challenging at the NMJ, given the resolution limit of the confocal system. The difference in Tkv distribution in σ 2-adaptin and *Rab11*

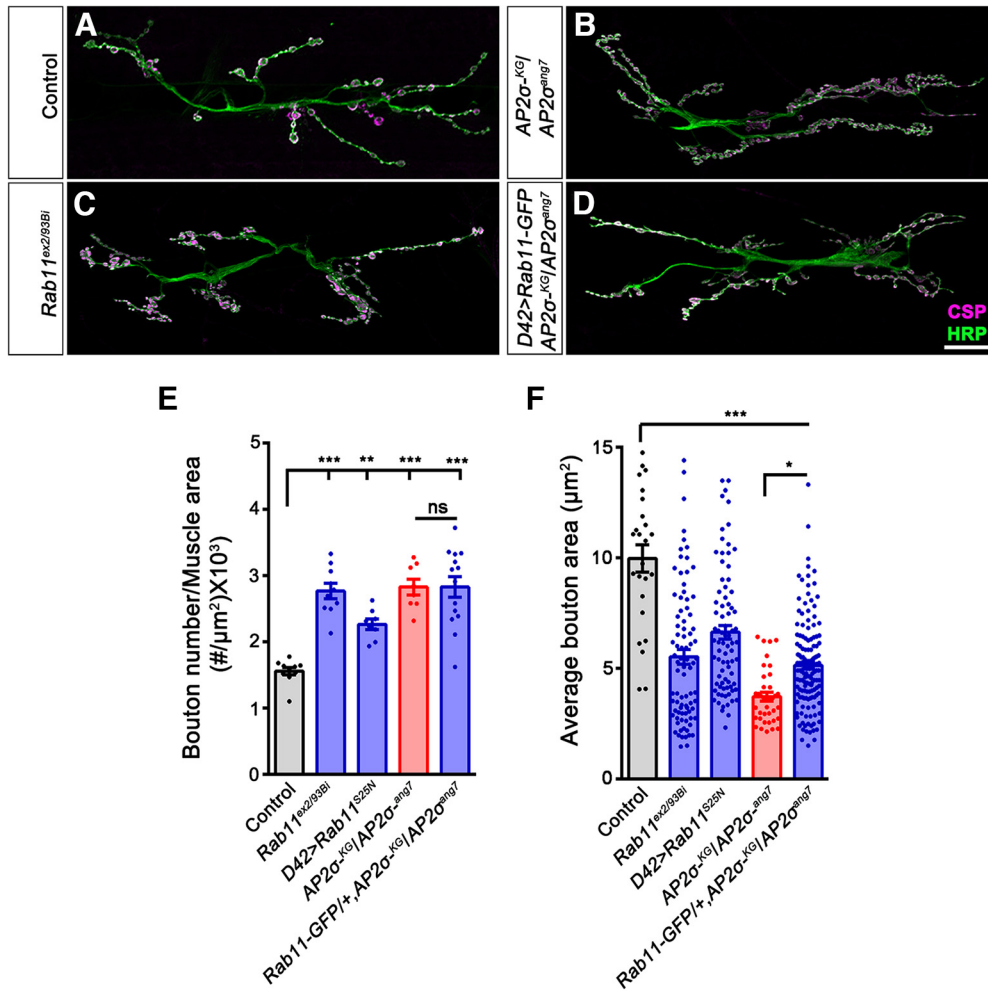


Figure 8. *Rab11* mutants phenocopy NMJ structural defects of $\sigma 2$ -*adaptin* mutation. **A–D**, Confocal images of NMJ synapses at muscle 6/7 NMJ at A2 hemisegment in control (**A**), $AP2\sigma^{KG02457}/AP2\sigma^{ang7}$ (**B**), *Rab11^{ex2/93 Bi}* (**C**), and *D42-Gal4>YFP-Rab11^{S25N}* (**D**) double immunolabeled with a presynaptic synaptic vesicle marker, CSP (magenta), and a neuronal membrane marker, HRP (green), to mark the bouton outline. Scale bar in **D** represents 20 μm . **E**, Histogram showing average bouton number normalized to the muscle area from muscle 6/7 NMJ at A2 hemisegment in control (1.56 ± 0.06), *Rab11^{ex2/93 Bi}* (2.77 ± 0.11), *D42-Gal4*-driven dominant-negative *YFP-Rab11^{S25N}* (2.26 ± 0.08), $AP2\sigma^{KG02457}/AP2\sigma^{ang7}$ (2.83 ± 0.12), and *UAS-YFP-Rab11^{WT}/+; D42-Gal4, AP2 σ^{ang7} /AP2 $\sigma^{KG02457}$* (2.83 ± 0.16). Error bar represents SEM; statistical analysis was done using one-way ANOVA followed by *post hoc* Tukey’s test. $***p < 0.001$, $*p < 0.05$; ns, not significant. **F**, Histogram showing average bouton area from muscle 6/7 NMJ at A2 hemisegment in control (9.97 ± 0.62), *Rab11^{ex2/93 Bi}* (5.51 ± 0.33), *D42-Gal4*-driven dominant-negative *YFP-Rab11^{S25N}* (6.63 ± 0.31), $AP2\sigma^{KG02457}/AP2\sigma^{ang7}$ (3.71 ± 0.2), and *UAS-YFP-Rab11^{WT}/+; D42-Gal4, AP2 σ^{ang7} /AP2 $\sigma^{KG02457}$* (5.14 ± 0.17). Error bar represents SEM; statistical analysis was done using one-way ANOVA followed by *post hoc* Tukey’s test. $***p < 0.001$, $*p < 0.05$; ns, not significant. Data supporting that expression of wild-type or constitutive active Rab11 does not alter NMJ morphology and does not restore NMJ morphologic defects of $\sigma 2$ -*adaptin* mutants is shown in Extended Data Figures 8-1 and 8-2, respectively. Data supporting that expression of wild-type or dominant negative Rab11 and constitutive active Rab11 does not restore the functional defects of $\sigma 2$ -*adaptin* mutants is shown in Extended Data Figures 8-3 and 8-4, respectively.

mutants also argues for additional pathways, other than Rab11, through which $\sigma 2$ -*adaptin* may regulate BMP signaling.

Tkv receptors in $\sigma 2$ -*adaptin* mutants could be accumulated either at the plasma membrane because of inefficient CME or at the early endosomes caused by inefficient recycling. If Tkv were accumulated at the early endosomes, we would expect greater colocalization with Rab5, which is not the case. However, based on reduced Rab11 staining at the $\sigma 2$ -*adaptin* mutant synapses, we conclude that the portion of the receptors

in Rab5 positive early endosomes fail to recycle back to the plasma membrane. This conclusion also fits with previous observations that defective CME results in the accumulation of endosome-like structures in cultured hippocampal neurons (Kononenko et al., 2014) and is substantiated by our electron microscopy data. The link between clathrin-mediated dynamin-dependent endocytosis and BMP signaling is still a contentious topic. A recent study using human umbilical vein endothelial cells (HUVECs) has shown that treating these cells with BMP-9 triggered Caveolin-1 and dynamin-2-mediated

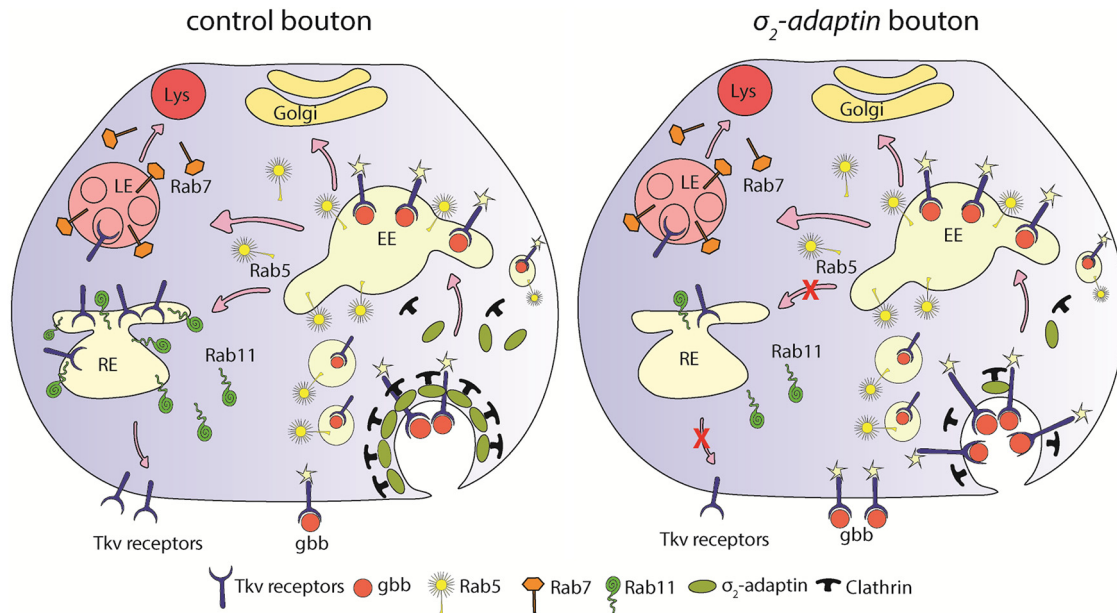


Figure 9. Model depicting the role of $\sigma 2$ -adaptin in BMP receptor trafficking at the NMJ. The model depicts a novel function of $\sigma 2$ -adaptin/AP2 in Tkv receptor trafficking at the *Drosophila* NMJ. Retrograde NMJ growth signaling in *Drosophila* involves Gbb ligand that is secreted from postsynaptic muscles and binds to BMP receptors on the presynaptic membrane to activate them (Aberle et al., 2002; McCabe et al., 2003). Activated receptors are then internalized through CME and fuse with early endosomes to trigger the downstream signaling cascade (Hartung et al., 2006). From early endosomes, receptors either get sorted to the Rab11-positive recycling endosomes that recycle them back to the presynaptic membrane or are sorted for lysosomal degradation (Liu et al., 2014; Deshpande and Rodal, 2016). Depletion of $\sigma 2$ -adaptin/AP2-complex leads to enrichment of Tkv receptors at the presynaptic membrane and/or in the early endosomes leading to elevated BMP signaling resulting in synaptic overgrowth. It is also likely that reduced synaptic Rab11 levels in $\sigma 2$ -adaptin might perturb Rab11-mediated recycling of Tkv leading to enhanced BMP-signaling.

endocytosis of its receptor, activin-like kinase 1 (ALK-1). Surprisingly, this ALK-1 endocytosis was not mediated by Clathrin heavy chain (Tao et al., 2020). At the *Drosophila* NMJ, endocytosis attenuates BMP signaling (O'Connor-Giles et al., 2008), whereas in *Drosophila* wing discs and intestinal stem cells, endocytosis facilitates the signaling cascade by internalizing Tkv (Gui et al., 2016; Tracy Cai et al., 2019), pointing toward a tissue-specific mechanism. Our results suggest a model where bulk membrane endocytosis is insufficient in removing Tkv from the plasma membrane; besides, the synapses in $\sigma 2$ -adaptin mutants fail to recycle remaining receptors from early endosomes leading to enhanced signaling and NMJ growth defects.

Functional and morphologic aspects of $\sigma 2$ -adaptin-mediated BMP signaling can be discriminated

Morphologic features of synapses often dictate functional outcomes, and physiological analyses of BMP signaling mutants reveal the same. In *wit* mutants, the size of the NMJ is significantly reduced with concomitant reduced evoked excitatory potentials (Aberle et al., 2002; Marqués et al., 2002). Analyses of *tkv* and *sax*, co-Smad *Medea*, and transcription factor *Mad* showed that these NMJs have smaller synapses with severe functional deficits (McCabe et al., 2004). Consistent with the role of BMP-signaling in regulating NMJ growth, *gbb* mutant larvae also exhibit shorter NMJs with severely reduced

evoked potentials (McCabe et al., 2003). $\sigma 2$ -adaptin mutant synapses show a modest reduction in evoked potentials, and the protein is dispensable for maintaining basal synaptic transmission (Choudhury et al., 2016). However, a rundown of EJP amplitudes during high-frequency stimulation in synaptic mutants implicated in CME, such as *Endo*, *Synj*, and *Dap160*, show a rapid stimulus-dependent decline in EJP amplitude that recovers following a period of rest after the high-frequency stimulation paradigm (Verstreken et al., 2003; Koh et al., 2004). In our previous study, we reported that $\sigma 2$ -adaptin mutants do not recover from synaptic depression even after the 90s rest after the cessation of high-frequency stimulation (Choudhury et al., 2016). This observation suggested that in addition to its requirement in synaptic membrane retrieval, the $\sigma 2$ -adaptin function is also required during the much slower process of SV trafficking, possibly at one of the rate-limiting steps in SV regeneration. This conclusion is supported by our EM data that shows the accumulation of endosome-like structures more frequently at the mutant synapses when compared with *w¹¹¹⁸* controls. EJP and high-frequency recordings from $\sigma 2$ -adaptin mutant synapses with one copy of *tkv⁷* did not show any rescue in synaptic function. These data drive the conclusion that partial reduction of BMP pathway components can only rescue morphologic defects in $\sigma 2$ -adaptin mutants but not functional aspects and that morphologic and functional deficits can be discriminated in these mutants. Besides, the partial rescue of bouton size and bouton

clustering at the NMJ argues for possible deregulation of multiple signaling pathways in $\sigma 2$ -*adaptin* mutants that remain to be explored.

Our study uncovers and extends the existing knowledge of synaptic growth signaling and endocytosis. We provide four lines of evidence on the critical role of $\sigma 2$ -*adaptin* in modulating BMP-dependent synaptic growth signaling at the *Drosophila* NMJ. First, we show using genetics that the morphologic defects in $\sigma 2$ -*adaptin* mutant synapses can be partially rescued by introducing a mutant copy of the BMP receptors, *tkv*, and *wit*. We also show a direct epistatic interaction between $\sigma 2$ -*adaptin* and the inhibitory Smad, Dad. Second, using immunohistochemistry, we show that $\sigma 2$ -*adaptin* mutant synapses accumulate Tkv at the plasma membrane and some of these receptors that are endocytosed and make it to the early endosomes fail to recycle back to the plasma membrane. Third, our electrophysiology data establish that morphologic and functional defects can be discriminated in $\sigma 2$ -*adaptin* mutants. Finally, our electron micrographs provide evidence for the presence of large endosomes and support our conclusion that $\sigma 2$ -*adaptin* is critically required at a later step of vesicle regeneration following endocytosis from the plasma membrane.

While this study does not report a direct biochemical or epistatic interaction between $\sigma 2$ -*adaptin* and Rab11, we observed a significant reduction in Rab11 immunoreactivity in $\sigma 2$ -*adaptin* mutant synapses that could be restored by neuronal expression of $\sigma 2$ -*adaptin* transgenes. However, the structural and functional defects of $\sigma 2$ -*adaptin* mutants could not be restored by neuronal expression of Rab11^{WT} or Rab11^{CA}. This rules out the notion that $\sigma 2$ -*adaptin* phenotypes result from the observed reduction of Rab11. The *Rab11* mutant used in this study is a hypomorph with substantial Rab11 protein being detected by us and others (Khodosh et al., 2006). This precludes further epistatic analyses of this mutant. The fact that Rab11 protein could still be detected in these *Rab11* hypomorphic mutants may explain why pMad levels were not as upregulated when compared with $\sigma 2$ -*adaptin* mutants. Finally, the separation of Tkv immunoreactivity from the synaptic membrane versus that of the endosomal membrane is challenging, given the resolution of the imaging system used here. Our electron micrographs, however, convincingly show an accumulation of endosome-like structures close to the plasma membrane in $\sigma 2$ -*adaptin* mutant boutons. The endosome-like structures observed in the $\sigma 2$ -*adaptin* mutants are strikingly similar to structures previously reported for clathrin (Khodosh et al., 2006), AP180 (B Zhang et al., 1998), and Rab11 (Inoshita et al., 2017), among others. Thus, Tkv receptors could likely be enriched in these endosome-like compartments.

We propose a model in which $\sigma 2$ -*adaptin*/AP2-complex is required for the attenuation of BMP signaling at the *Drosophila* NMJ. In the absence of AP2, recycling of Tkv is compromised, which results in its enrichment at the presynaptic membrane and/or in the early endosomes leading to elevated BMP signaling and synaptic overgrowth (Fig. 9). This study thus opens new avenues where

the role of other CME components and their interaction with various growth signaling pathways can be studied. Since receptor localization and regulation appear to be the central theme in modulating BMP signaling and synapse growth, it will be interesting to perform structure-function analyses of BMP receptors and identify key residues/motifs that interact with AP2 and facilitate its endocytosis. Mutating tyrosine-based signal (YXX ϕ) and dileucine-based signal ([DE]XXXL[L/I]) motifs in Tkv and Wit could lead to further understanding of these intricate interactions.

References

- Aberle H, Haghghi AP, Fetter RD, McCabe BD, Magalhães TR, Goodman CS (2002) wishful thinking encodes a BMP type II receptor that regulates synaptic growth in *Drosophila*. *Neuron* 33:545–558.
- Ayyaz A, Li H, Jasper H (2015) Haemocytes control stem cell activity in the *Drosophila* intestine. *Nat Cell Biol* 17:736–748.
- Ball RW, Warren-Paquin M, Tsurudome K, Liao EH, Elazzouzi F, Cavanagh C, An BS, Wang TT, White JH, Haghghi AP (2010) Retrograde BMP signaling controls synaptic growth at the NMJ by regulating trio expression in motor neurons. *Neuron* 66:536–549.
- Budnik V, Salinas PC (2011) Wnt signaling during synaptic development and plasticity. *Curr Opin Neurobiol* 21:151–159.
- Chavrier P, Parton RG, Hauri HP, Simons K, Zerial M (1990) Localization of low molecular weight GTP binding proteins to exocytic and endocytic compartments. *Cell* 62:317–329.
- Choudhury SD, Mushtaq Z, Reddy-Alla S, Balakrishnan SS, Thakur RS, Krishnan KS, Raghu P, Ramaswami M, Kumar V (2016) $\sigma 2$ -*Adaptin* facilitates basal synaptic transmission and is required for regenerating endo-exo cycling pool under high-frequency nerve stimulation in *Drosophila*. *Genetics* 203:369–385.
- Collins CA, Wairkar YP, Johnson SL, DiAntonio A (2006) Highwire restrains synaptic growth by attenuating a MAP kinase signal. *Neuron* 51:57–69.
- Cosker KE, Segal RA (2014) Neuronal signaling through endocytosis. *Cold Spring Harb Perspect Biol* 6:a020669.
- Deivasigamani S, Basargekar A, Shweta K, Sonavane P, Ratnaparkhi GS, Ratnaparkhi A (2015) A presynaptic regulatory system acts transsynaptically via Mon1 to regulate glutamate receptor levels in *Drosophila*. *Genetics* 201:651–664.
- Deshpande M, Rodal AA (2016) The crossroads of synaptic growth signaling, membrane traffic and neurological disease: insights from *Drosophila*. *Traffic* 17:87–101.
- Dickman DK, Lu Z, Meinertzhagen IA, Schwarz TL (2006) Altered synaptic development and active zone spacing in endocytosis mutants. *Curr Biol* 16:591–598.
- Di Fiore PP, De Camilli P (2001) Endocytosis and signaling. an inseparable partnership. *Cell* 106:1–4.
- Dubois L, Lecourtois M, Alexandre C, Hirst E, Vincent JP (2001) Regulated endocytic routing modulates wingless signaling in *Drosophila* embryos. *Cell* 105:613–624.
- Dunn KW, McGraw TE, Maxfield FR (1989) Iterative fractionation of recycling receptors from lysosomally destined ligands in an early sorting endosome. *J Cell Biol* 109:3303–3314.
- Franco B, Bogdanik L, Bobinnec Y, Debec A, Bockaert J, Parmentier ML, Grau Y (2004) Shaggy, the homolog of glycogen synthase kinase 3, controls neuromuscular junction growth in *Drosophila*. *J Neurosci* 24:6573–6577.
- Goold CP, Davis GW (2007) The BMP ligand Gbb gates the expression of synaptic homeostasis independent of synaptic growth control. *Neuron* 56:109–123.
- Gruenberg J, Griffiths G, Howell KE (1989) Characterization of the early endosome and putative endocytic carrier vesicles in vivo and with an assay of vesicle fusion in vitro. *J Cell Biol* 108:1301–1316.

- Guan Z, Quiñones-Frías MC, Akbergenova Y, Littleton JT (2020) *Drosophila* Synaptotagmin 7 negatively regulates synaptic vesicle release and replenishment in a dosage-dependent manner. *Elife* 9:e55443.
- Gui J, Huang Y, Shimmi O (2016) Scribbled optimizes BMP signaling through its receptor internalization to the Rab5 endosome and promote robust epithelial morphogenesis. *PLoS Genet* 12:e1006424.
- Hartung A, Bitton-Worms K, Rechtman MM, Wenzel V, Boergermann JH, Hassel S, Henis YI, Knaus P (2006) Different routes of bone morphogenic protein (BMP) receptor endocytosis influence BMP signaling. *Mol Cell Biol* 26:7791–7805.
- Horgan CP, McCaffrey MW (2011) Rab GTPases and microtubule motors. *Biochem Soc Trans* 39:1202–1206.
- Inoshita T, Arano T, Hosaka Y, Meng H, Umezaki Y, Kosugi S, Morimoto T, Koike M, Chang HY, Imai Y, Hattori N (2017) Vps35 in cooperation with LRRK2 regulates synaptic vesicle endocytosis through the endosomal pathway in *Drosophila*. *Hum Mol Genet* 26:2933–2948.
- Joseph BB, Wang Y, Edeen P, Lazdović V, Grant BD, Fay DS (2020) Control of clathrin-mediated endocytosis by NIMA family kinases. *PLoS Genet* 16:e1008633.
- Jovic M, Sharma M, Rahajeng J, Caplan S (2010) The early endosome: a busy sorting station for proteins at the crossroads. *Histol Histopathol* 25:99–112.
- Kadlecova Z, Spielman SJ, Loerke D, Mohanakrishnan A, Reed DK, Schmid SL (2017) Regulation of clathrin-mediated endocytosis by hierarchical allosteric activation of AP2. *J Cell Biol* 216:167–179.
- Kasprowicz J, Kuenen S, Miskiewicz K, Habets RL, Smits L, Verstreken P (2008) Inactivation of clathrin heavy chain inhibits synaptic recycling but allows bulk membrane uptake. *J Cell Biol* 182:1007–1016.
- Kawasaki F, Iyer J, Posey LL, Sun CE, Mammen SE, Yan H, Ordway RW (2011) The DISABLED protein functions in CLATHRIN-mediated synaptic vesicle endocytosis and exocytotic coupling at the active zone. *Proc Natl Acad Sci U S A* 108:E222–E229.
- Kelly EE, Horgan CP, Goud B, McCaffrey MW (2012) The Rab family of proteins: 25 years on. *Biochem Soc Trans* 40:1337–1347.
- Keshishian H, Kim YS (2004) Orchestrating development and function: retrograde BMP signaling in the *Drosophila* nervous system. *Trends Neurosci* 27:143–147.
- Khodosh R, Augsburger A, Schwarz TL, Garrity PA (2006) Bchs, a BEACH domain protein, antagonizes Rab11 in synapse morphogenesis and other developmental events. *Development* 133:4655–4665.
- Kim NC, Marqués G (2012) The Ly6 neurotoxin-like molecule target of wit regulates spontaneous neurotransmitter release at the developing neuromuscular junction in *Drosophila*. *Dev Neurobiol* 72:1541–1558.
- Koh TW, Verstreken P, Bellen HJ (2004) Dap160/intersectin acts as a stabilizing scaffold required for synaptic development and vesicle endocytosis. *Neuron* 43:193–205.
- Kononenko NL, Puchkov D, Classen GA, Walter AM, Pechstein A, Sawade L, Kaempf N, Trimbuch T, Lorenz D, Rosenmund C, Maritzen T, Haucke V (2014) Clathrin/AP-2 mediate synaptic vesicle reformation from endosome-like vacuoles but are not essential for membrane retrieval at central synapses. *Neuron* 82:981–988.
- Liu Z, Huang Y, Hu W, Huang S, Wang Q, Han J, Zhang YQ (2014) dAcl1, the *Drosophila* ortholog of acyl-CoA synthetase long-chain family member 3 and 4, inhibits synapse growth by attenuating bone morphogenetic protein signaling via endocytic recycling. *J Neurosci* 34:2785–2796.
- Lloyd TE, Atkinson R, Wu MN, Zhou Y, Pennetta G, Bellen HJ (2002) Hrs regulates endosome membrane invagination and tyrosine kinase receptor signaling in *Drosophila*. *Cell* 108:261–269.
- López-Hernández T, Takenaka K-i, Mori Y, Kongpracha P, Nagamori S, Haucke V, Takamori S (2021) Clathrin-independent endocytic retrieval of SV proteins mediated by the clathrin adaptor AP-2 at mammalian central synapses. *bioRxiv*. doi: 10.1101/2021.06.24.449713.
- Marqués G, Bao H, Haerry TE, Shimell MJ, Duchek P, Zhang B, O'Connor MB (2002) The *Drosophila* BMP type II receptor Wishful Thinking regulates neuromuscular synapse morphology and function. *Neuron* 33:529–543.
- McCabe BD, Marqués G, Haghighi AP, Fetter RD, Crotty ML, Haerry TE, Goodman CS, O'Connor MB (2003) The BMP homolog Gbb provides a retrograde signal that regulates synaptic growth at the *Drosophila* neuromuscular junction. *Neuron* 39:241–254.
- McCabe BD, Hom S, Aberle H, Fetter RD, Marques G, Haerry TE, Wan H, O'Connor MB, Goodman CS, Haghighi AP (2004) Highwire regulates presynaptic BMP signaling essential for synaptic growth. *Neuron* 41:891–905.
- Mitchell H, Choudhury A, Pagano RE, Leof EB (2004) Ligand-dependent and -independent transforming growth factor-beta receptor recycling regulated by clathrin-mediated endocytosis and Rab11. *Mol Biol Cell* 15:4166–4178.
- Mottola G, Classen AK, González-Gaitán M, Eaton S, Zerial M (2010) A novel function for the Rab5 effector Rabenosyn-5 in planar cell polarity. *Development* 137:2353–2364.
- Nahm M, Long AA, Paik SK, Kim S, Bae YC, Broadie K, Lee S (2010) The Cdc42-selective GAP rich regulates postsynaptic development and retrograde BMP transsynaptic signaling. *J Cell Biol* 191:661–675.
- O'Connor-Giles KM, Ho LL, Ganetzky B (2008) Nervous wreck interacts with thickveins and the endocytic machinery to attenuate retrograde BMP signaling during synaptic growth. *Neuron* 58:507–518.
- Papagiannouli F, Berry CW, Fuller MT (2019) The Dlg module and clathrin-mediated endocytosis regulate EGFR signaling and cyst cell-germline coordination in the *Drosophila* testis. *Stem Cell Reports* 12:1024–1040.
- Persson U, Izumi H, Souchelnytskyi S, Itoh S, Grimsby S, Engström U, Heldin CH, Funa K, ten Dijke P (1998) The L45 loop in type I receptors for TGF-beta family members is a critical determinant in specifying Smad isoform activation. *FEBS Lett* 434:83–87.
- Piccioli ZD, Littleton JT (2014) Retrograde BMP signaling modulates rapid activity-dependent synaptic growth via presynaptic LIM kinase regulation of cofilin. *J Neurosci* 34:4371–4381.
- Rikhy R, Kumar V, Mittal R, Krishnan KS (2002) Endophilin is critically required for synapse formation and function in *Drosophila melanogaster*. *J Neurosci* 22:7478–7484.
- Rodal AA, Motola-Barnes RN, Littleton JT (2008) Nervous wreck and Cdc42 cooperate to regulate endocytic actin assembly during synaptic growth. *J Neurosci* 28:8316–8325.
- Rodal AA, Blunk AD, Akbergenova Y, Jorquera RA, Buhl LK, Littleton JT (2011) A presynaptic endosomal trafficking pathway controls synaptic growth signaling. *J Cell Biol* 193:201–217.
- Sanyal S (2009) Genomic mapping and expression patterns of C380, OK6 and D42 enhancer trap lines in the larval nervous system of *Drosophila*. *Gene Expr Patterns* 9:371–380.
- Schwartz SL, Cao C, Pylpenko O, Rak A, Wandinger-Ness A (2007) Rab GTPases at a glance. *J Cell Sci* 120:3905–3910.
- Shi W, Chen Y, Gan G, Wang D, Ren J, Wang Q, Xu Z, Xie W, Zhang YQ (2013) Brain tumor regulates neuromuscular synapse growth and endocytosis in *Drosophila* by suppressing mad expression. *J Neurosci* 33:12352–12363.
- Shimizu H, Kawamura S, Ozaki K (2003) An essential role of Rab5 in uniformity of synaptic vesicle size. *J Cell Sci* 116:3583–3590.
- Smith RB, Machamer JB, Kim NC, Hays TS, Marqués G (2012) Relay of retrograde synaptogenic signals through axonal transport of BMP receptors. *J Cell Sci* 125:3752–3764.
- Sorvina A, Shandala T, Brooks DA (2016) *Drosophila* Pkaap regulates Rab4/Rab11-dependent traffic and Rab11 exocytosis of innate immune cargo. *Biol Open* 5:678–688.
- Sulkowski MJ, Han TH, Ott C, Wang Q, Verheyen EM, Lippincott-Schwartz J, Serpe M (2016) A novel, noncanonical BMP pathway modulates synapse maturation at the *Drosophila* neuromuscular junction. *PLoS Genet* 12:e1005810.

- Sweeney ST, Davis GW (2002) Unrestricted synaptic growth in spinster-a late endosomal protein implicated in TGF-beta-mediated synaptic growth regulation. *Neuron* 36:403–416.
- Tanaka T, Nakamura A (2008) The endocytic pathway acts downstream of Oskar in *Drosophila* germ plasm assembly. *Development* 135:1107–1117.
- Tao B, Kraehling JR, Ghaffari S, Ramirez CM, Lee S, Fowler JW, Lee WL, Fernandez-Hernando C, Eichmann A, Sessa WC (2020) BMP-9 and LDL crosstalk regulates ALK-1 endocytosis and LDL transcytosis in endothelial cells. *J Biol Chem* 295:18179–18188.
- Tracy Cai X, Li H, Safyan A, Gawlik J, Pyrowolakis G, Jasper H (2019) AWD regulates timed activation of BMP signaling in intestinal stem cells to maintain tissue homeostasis. *Nat Commun* 10:2988.
- Ullrich O, Reinsch S, Urbé S, Zerial M, Parton RG (1996) Rab11 regulates recycling through the pericentriolar recycling endosome. *J Cell Biol* 135:913–924.
- Vanlandingham PA, Fore TR, Chastain LR, Royer SM, Bao H, Reist NE, Zhang B (2013) Epsin 1 promotes synaptic growth by enhancing BMP signal levels in motoneuron nuclei. *PLoS One* 8:e65997.
- Verstreken P, Kjaerulf O, Lloyd TE, Atkinson R, Zhou Y, Meinertzhagen IA, Bellen HJ (2002) Endophilin mutations block clathrin-mediated endocytosis but not neurotransmitter release. *Cell* 109:101–112.
- Verstreken P, Koh TW, Schulze KL, Zhai RG, Hiesinger PR, Zhou Y, Mehta SQ, Cao Y, Roos J, Bellen HJ (2003) Synaptojanin is recruited by endophilin to promote synaptic vesicle uncoating. *Neuron* 40:733–748.
- Vuilleumier R, Lian T, Flibotte S, Khan ZN, Fuchs A, Pyrowolakis G, Allan DW (2019) Retrograde BMP signaling activates neuronal gene expression through widespread deployment of a conserved BMP-responsive cis-regulatory activation element. *Nucleic Acids Res* 47:679–699.
- Wang X, Shaw WR, Tsang HT, Reid E, O’Kane CJ (2007) *Drosophila* spichthyn inhibits BMP signaling and regulates synaptic growth and axonal microtubules. *Nat Neurosci* 10:177–185.
- Watanabe S, Trimbuch T, Camacho-Pérez M, Rost BR, Brokowski B, Söhl-Kielczynski B, Felies A, Davis MW, Rosenmund C, Jorgensen EM (2014) Clathrin regenerates synaptic vesicles from endosomes. *Nature* 515:228–233.
- West RJ, Lu Y, Marie B, Gao FB, Sweeney ST (2015) Rab8, POSH, and TAK1 regulate synaptic growth in a *Drosophila* model of frontotemporal dementia. *J Cell Biol* 208:931–947.
- Yeh E, Gustafson K, Boulianne GL (1995) Green fluorescent protein as a vital marker and reporter of gene expression in *Drosophila*. *Proc Natl Acad Sci U S A* 92:7036–7040.
- Zhang B, Koh YH, Beckstead RB, Budnik V, Ganetzky B, Bellen HJ (1998) Synaptic vesicle size and number are regulated by a clathrin adaptor protein required for endocytosis. *Neuron* 21:1465–1475.
- Zhang XW, Rui ML, Gan GM, Huang C, Yi JK, Lv HH, Xie W (2017) Neuroligin 4 regulates synaptic growth via the bone morphogenetic protein (BMP) signaling pathway at the *Drosophila* neuromuscular junction. *J Biol Chem* 292:17991–18005.
- Zhao G, Wu Y, Du L, Li W, Xiong Y, Yao A, Wang Q, Zhang YQ (2015) *Drosophila* S6 Kinase like inhibits neuromuscular junction growth by downregulating the BMP receptor thickveins. *PLoS Genet* 11:e1004984.
- Zhao L, Wang D, Wang Q, Rodal AA, Zhang YQ (2013) *Drosophila* cyfip regulates synaptic development and endocytosis by suppressing filamentous actin assembly. *PLoS Genet* 9:e1003450.